APPROVAL SHEET

Title of Thesis: EVALUATION OF HYDROGEN PEROXIDE-BASED OXIDATION ON THE MECHANICAL BEHAVIOUR OF ARTERIAL ELASTIN

Name of Candidate: Alexander Lacey

Master of Science, 2019

Thesis and Abstract Approved: _____

Dr. L.D.T. Topoleski

Professor

Mechanical Engineering Department

Date Approved: 18 June 2019

ABSTRACT

Title of Document: EVALUATION OF HYDROGEN PEROXIDE-BASED OXIDATION ON THE MECHANICAL BEHAVIOUR OF ARTERIAL ELASTIN

Alexander Lacey, M.S., 2019

Directed By: Dr. L.D.T. Topoleski, Mechanical Engineering Department, UMBC

Damage to the cardiovascular system, and associated cardiovascular diseases, is one of the leading causes of death in the world. Part of this damage may be caused by oxidative stress in the artery wall, which is associated with mechanical changes of the artery. In this thesis we examine the effect of oxidation caused by hydrogen peroxide (H_2O_2) on elastin isolated from porcine aortas.

Porcine arterial samples were obtained from a local butcher and cut into dog-bone-shaped specimens. The specimens were treated with a CNBr protocol to isolate the elastin. The elastin specimens were separated into 10 groups of 5 samples each. The samples were treated in 3% H_2O_2 from 5 minutes to 24 hours, with a control group excluded from the H_2O_2 treatment. The Biomechanical Materials Testing System (BiMaTS) was used to

monotonically load the specimens in tension to failure. Force and displacement data were recorded. These data were used to calculate stress and stretch ratio results. The maximum stress and stretch at maximum stress was determined for each specimen tested.

One-way ANOVA with Tukey HSD and Bland-Altman plots were used to evaluate the maximum stress and stretch at maximum stress results. It was determined that there was no statistically significant change in the maximum stress or the stretch at that maximum stress of elastin from exposure to H_2O_2.

EVALUATION OF HYDROGEN PEROXIDE-BASED OXIDATION ON THE MECHANICAL BEHAVIOUR OF ARTERIAL ELASTIN

By

Alexander Lacey

Thesis submitted to the Faculty of the Graduate School of the University of Maryland, Baltimore County, in partial fulfilment of the requirements for the degree of

Masters of Science

2019

Table of Contents

1.0 Introduction

The cardiovascular system is responsible for the distribution of nutrients and oxygen throughout the body. As one of the core anatomical systems, understanding its operation is critical to reducing disease in humans. In 2017, diseases of the cardiovascular system made up the top cause of death in the United States [1]. In this category of disease, the most prevalent form is arteriosclerosis, which encompasses all cardiovascular disease that damages the interior of the artery.

The primary goal of this thesis was to evaluate the effect of hydrogen peroxide (H_2O_2) on the material properties of arterial elastin. This goal was achieved by isolating the elastin using a method developed by Lu et. al [2], then treating the samples with H_2O_2 for a wide range of times. Mechanical testing of the treated samples was used to obtain Stress/Stretch curves of the elastin and investigate if the maximum stress value or stretch at that maximum stress changed with respect to the H_2O_2 treatment. Additionally, this response data was compared with existing oxidation experiment data to confirm validity of the experiment and have an established comparison point.

This thesis is organized into three major sections, a Background section discussing the relevant anatomical information and a literature review of similar research, a Methods section covering the processes used in the experiment, and a Results and Discussion section covering the data gathered by the experiment, the interpretation of the data, and how it compared to the existing data covered in the Background section.

2.0 Background

2.1 Circulatory Anatomy

The circulatory system is comprised of a closed loop of the heart with a network of arteries, veins, and capillaries arranged to distribute blood throughout the body. The heart's operation produces a pressure gradient that forces blood to travel through the circulatory system, creating a localized high-pressure environment that decreases in pressure as the blood travels further from the heart and splits into the smaller arteries, arterioles, and capillaries [3]. A schematic of this system is shown in Figure 1[4]. The circulatory system's purpose is to distribute oxygen and nutrients through the body, as well as remove waste and circulate elements of the immune system. The arterial side of this loop can be separated into two sub-sections,

the pulmonic, sending deoxygenated blood to the lungs, and the systemic, sending oxygenated blood through the rest of the body. The aorta is the primary systemic artery, leaving the heart and branching off into the other major arteries. The aorta can be divided into three major sections, the ascending aorta, the aortic arch, and the descending aorta, which in itself has sub-classifications as the artery descends down the thorax and separates into smaller blood vessels [3][5].

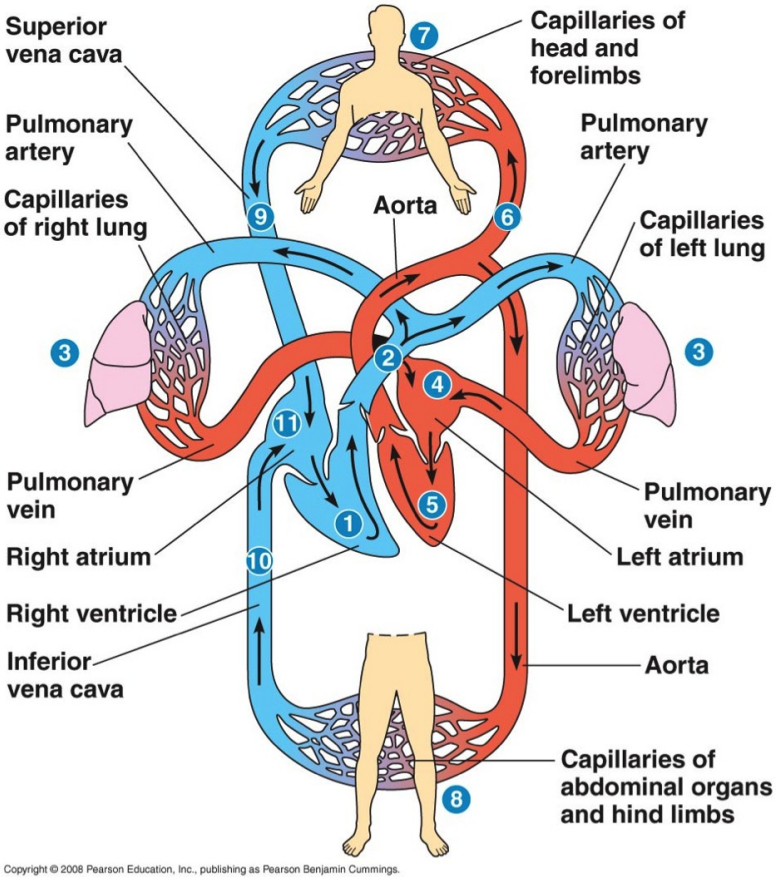

Figure 1: Schematic of the Cardiovascular System [4]

2.2 Arterial Anatomy

Arteries are structured to be able to withstand the pressure generated by the heart to move blood through the body. To achieve this, they are capable of elastically deforming because of abundant amounts of a protein called elastin (discussed in detail in section 2.5). As the blood moves further from the heart, the arteries become less elastic and more muscular in structure as the overall pressure decreases. The schematic shown in Figure 2 shows a general relationship of pressure and velocity of the blood as it cycles from the heart, through the arteries to the capillaries, then back through the veins. Healthy blood pressure has a systolic value of 120 mm of mercury (mmHg) with a diastolic value of 80mmHg [6]. The increase in muscular tissue in more distant arteries allows for regulation of blood pressure to maintain blood flow [3].

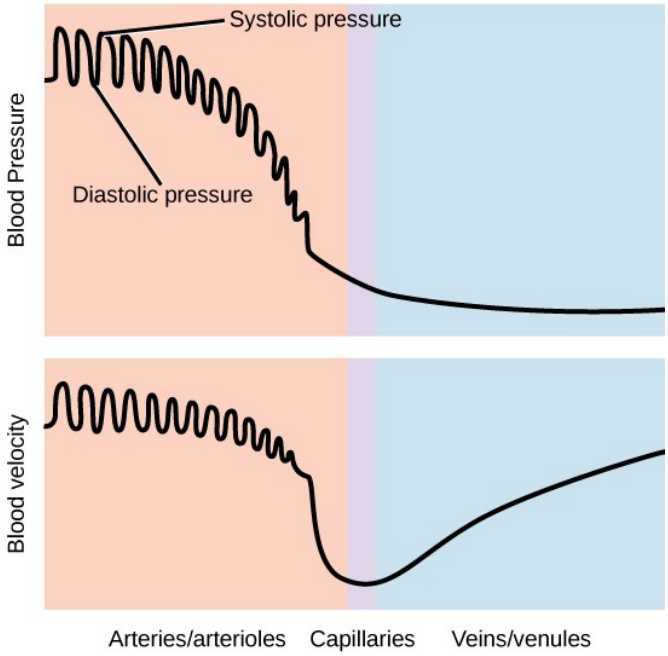

Figure 2: Schematic of Blood Pressure and Velocity Through the Circulatory System [6]

The artery can be described as a series of three major layers, the Adventitia, Media, and Intima. Figure 3 shows the layers as well as some of the important components of the artery to be discussed. The Adventitia is the outermost layer and is comprised of a dense scaffold of Type I collagen that supports elastin, nerves, the vaso vasorum, and fibroblasts [5]. Fibroblasts are cells that function to synthesize and regulate the amount of Type I collagen in the artery.

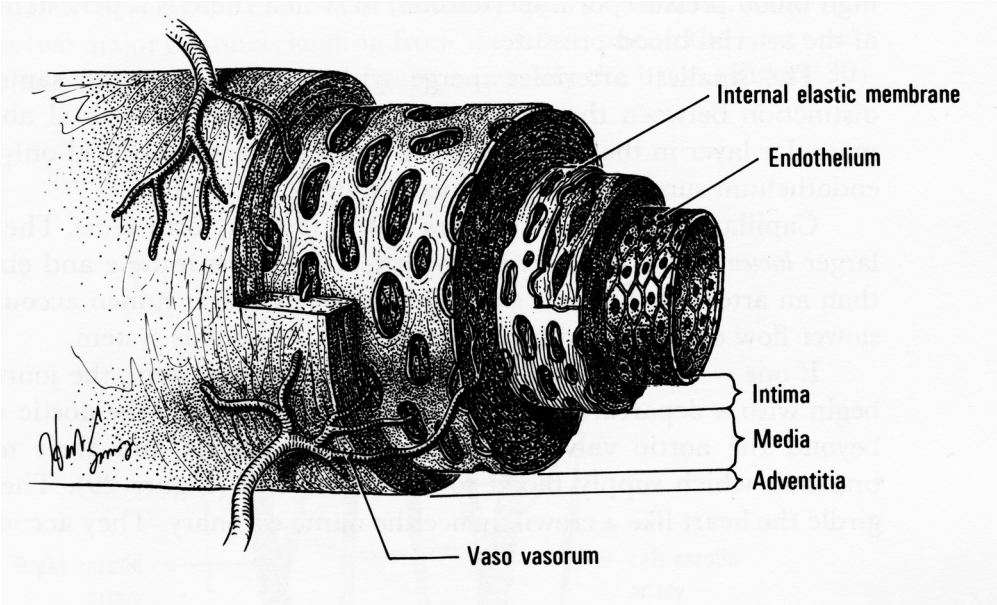

Figure 3: Major Layers and Tissues of the Artery [3]

The vaso vasorum is a network of capillaries, arterioles, and venules that provide nutrients and O_2 to the outer surfaces of arteries that are too thick for such transport from the internal surface [5]. In muscular arteries, such as the aorta, the Media is made up of radial layers of smooth muscle

cells supported by a lattice of Type I, III, and V collagen, and elastin. Each of these layers, which in elastic arteries are between 5 and 15 micrometers (μm) thick, are separated by porous sheets of elastin. The Intima is the thinnest of the layers, which for the aorta consists of only a layer of endothelial cells, a layer of smooth muscle cells, and a basal lamina. The basal lamina is a net of Type IV collagen with proteoglycans, Laminin, and Fibronectin molecules to provide adhesion to the endothelial cells [5]. Between each of these major layers are minor layers of basal lamina and endothelial cells, the internal elastic lamina between the Intima and Media, and the external elastic lamina between the Media and Adventita.

Damage to arterial tissues, excluding external trauma, is caused by arteriosclerosis, which encompasses a variety of tissue composition changes resulting in loss of elasticity of the artery wall. One such variation of tissue changes is atherosclerosis, which over time causes loss of elasticity through the formation of LDL cholesterol plaques in the Intima layer, which thickens the artery, obstructing blood flow both through the artery as well as into the artery itself [3][5]. This plaque accumulation has been tied to oxidative stress in the artery wall [7].

2.3 The Extracellular Matrix

The Extracellular Matrix (ECM) is a lattice of macro-molecules that serves as a framework to support cells to make up different tissues in the body. It serves to strengthen tissue and maintain structure while providing a biological scaffold for cells and proteins to adhere to [5]. The primary macro-molecule classes found in the ECM are collagen, elastin, proteoglycans, and structural glycoproteins [8]. Collagen and elastin are described in greater detail in the following sections because they have greater relevance to this thesis compared to proteoglycans and structural glycoproteins. The precise components found in the ECM depends on the particular location in the body, which to say indicates that specific proteins and structures discussed are in respect to arterial tissue and that the ECM structure and composition may differ elsewhere in the body.

Proteoglycans are a class of macro-molecules that consist of a core protein bound to at least one glycosaminoclycan side chain [8]. In the ECM there are three major sub-classes: leucine-rich, hyaluronate-binding, and collagenous. The collagenous sub-class contains types IX and XII collagen, which are associated with interacting with types II and I collagen respectively.

Structural glycoproteins are a class of macro-molecules that are defined as having at least one heterosaccharide chain [9]. Their structure indicates that they are both structural and functional in nature as well as possessing independent binding sites [8]. Some of the structural glycoproteins that are found in the vascular ECM are Fibrillin, Fibronectin, and Laminin [5][8]. Fibrillin is found as part of the elastin formation process, and is discussed in section 2.5. Fibronectin is noted as significant in adhering ECM proteins to other cells as well as in wound healing [10][11]. Laminin is found as a structural component in the basal lamina [12].

2.4 Collagen

The different types of collagen described previously are based on classifications of chemical structure of the protein, which then relate to the anatomical location, fibril arrangement, and type of synthesis cell [9]. Of these, there are over 15 [5][13] distinct varieties that are referenced, 6 of which are found in the Extracellular Matrix [5]: types I, III, IV, V, VI, and VIII. Of these, types I, III, IV, and V are covered in the previous description of arterial anatomy, leaving types VI and VIII to be discussed. Type VI collagen is found throughout the ECM found in muscular areas, primarily

serving to connect muscle cells to the ECM [14]. Type VIII collagen is synthesized by endothelial cells and is associated with the basement membrane in the Intima [15].

There is a noted discrepancy in the reporting of occurrence of collagen types in tissue, as the collagenous proteoglycan contains both types IX and XII as remarked previously. This can be attributed to difficulty in identifying different collagen types due to the soluble nature of the protein. In other literature, up to 28 varieties of collagen were noted [16], however a preliminary investigation into that number failed to identify any citable source that detailed each type and the differences between them. As the focus of this thesis is on the behaviour of elastin, not collagen, it was decided to focus on the types of collagen that relate to arteries only.

2.5 Elastin

Elastin is an insoluble support protein in connective tissue, notably different from collagen because of its high elasticity. It is formed from the precursor protein tropoelastin, synthesized as a soluble protein that cross-links into the insoluble form [8]. The insoluble elastin proteins are arranged in series of fibers held together with microfibrillar components to form

elastin fibrils [8]. Fibrillin is found as a component of these microfibrillar components in the elastin formation process. The elastin fibrils are bundled together into fibers along with other ground proteins and form the elastic portion of the ECM [17]. Decreased tissue elasticity is attributed to degradation of elastin, leading into dilation of the tissue and potentially mechanical failure through an aneurysm [18]. Elastin is reported to be inert to many protein solvents, making isolation of it fairly straightforward.

Elastin fiber alignment in the aorta depends on the layer in which the sheet is located. Elastin fibers in the internal elastic lamina are aligned parallel with blood flow, while elastin in the external elastic lamina and Media layers are aligned perpendicular to blood flow [19]. Figure 4 shows the Medial elastin sheet via confocal microscopy, aligned so that the direction of blood flow is along the vertical axis. It can be observed that the fibers exhibit a heavy directionality with the majority of the fibers arranged in an uniaxially way.

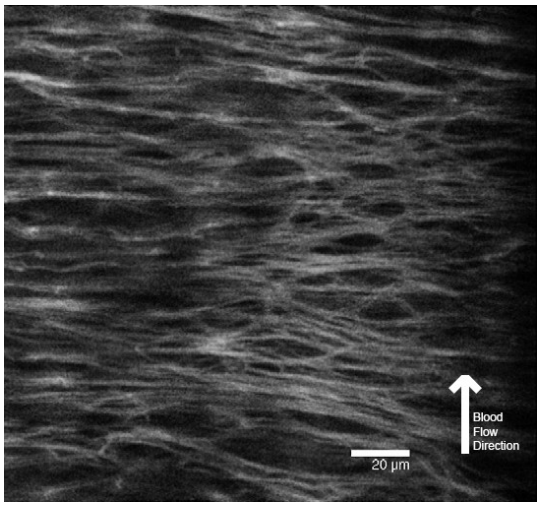

Figure 4: Confocal Microscopy of Medial Elastin Sheet [19]; Blood flow in vertical axis

Due to the durability and insolubility of elastin, multiple methods developed to isolate the protein from other tissues have been established. In no particular order, some of the established methods of isolating elastin are: using hot alkali [8][20], autoclaving [8][20], the procedure developed by B. Starcher using disodium phosphate and hydrogen chloride [8], and the procedure developed by Q. Lu using cyanogen bromide (CNBr) [2].

Elastin isolation using hot alkali involves heating cleaned tissue in NaOH at 100°C for 10 minutes, then centrifuging and rinsing the tissue [8]. Isolation through autoclaving is performed at 25psi and 121.1°C with samples in distilled water for a 45 minute cycle [21]. Both of these processes must be repeated multiple times to remove all soluble proteins. Mecham [21] reports that autoclaving produces less damage to the elastin protein, but more contaminants in the final samples. Starcher's elastin isolation procedure is a combination of autoclaving with a CNBr treatment to avoid degradation of elastin fibers while still keeping a high degree of tissue purity [8][21]. The CNBr treatment is the one used in the experimental portion of this research, and is discussed in detail in section 3.3. This method was chosen for two reasons. First, there is previous work from the same laboratory [22][23] using the CNBr treatment, and thus the procedure is

well-documented and all chemicals and equipment are available for use. Second, the other three methods are designed to isolate elastin in minced or powdered tissue samples, requiring additional steps to apply to larger specimens and verify that the isolation was completed correctly. The CNBr method can be applied to larger specimens, allowing for specific geometries to be maintained.

2.6 Hydrogen Peroxide

H_2O_2 is a commonly used chemical in dental and surgical applications, most typically in wound irrigation [24], tooth whitening [25], and disinfection [26]. H_2O_2 is commonly obtained in 30% and 3% concentrations, with its pure form appearing light blue in colour [26]. When used for wound irrigation, H_2O_2 is known for its antiseptic and antimicrobial effects. These effects are noted to be dependant on concentration, with lower concentrations having lesser and slower-acting effects [24]. H_2O_2 does pose the potential to cause damage to tissue, especially in tissue-forming cells such as osteoblasts and fibroblasts [26]. It is also noted to decompose into a significant volume of O_2, which can form into gas embolisms or in significant and sudden enough pressures cause mechanical tissue failure

[26]. High concentrations of H_2O_2 are also noted to have caustic effects on tissues. Lu et. al. [24] and Urban et. al. [26] both note that the effects of H_2O_2 toxicity, while present, are not more impactful than the benefits of treatment. Dental applications of H_2O_2 include irrigation and disinfection of wound areas after oral surgery as well as the prior-mentioned tooth whitening. The impact H_2O_2 has on tooth whitening was examined by Sulieman et. al. [25] via controlled staining with a tea solution, then through treatment with bleaching gel diluted to different levels of H_2O_2 concentration ranging from 5% to 35%. The number of bleaching gel applications required to obtain a uniform shade followed an inverse exponential relationship, where lower concentrations required more application periods.

In addition to the external introduction of H_2O_2 to the body, it is also found as part of intermediary cellular processes that produce reactive oxidative species (ROS) as part of their function. Most notably, H_2O_2 is produced in mitochondria as part of the O_2^- reduction cycle where O_2 enters the mitochondrial membrane, gains an electron, undergoes reaction into H_2O_2 through interaction with Manganese Superoxide Dismutase (Mn SOD), then leaves the mitochondrial membrane into the cell [27]. This reaction is

shown in Figure 5. H_2O_2 is also formed through NADPH oxidase, Cu SOD, Zn SOD, and lysyl oxidase [28].

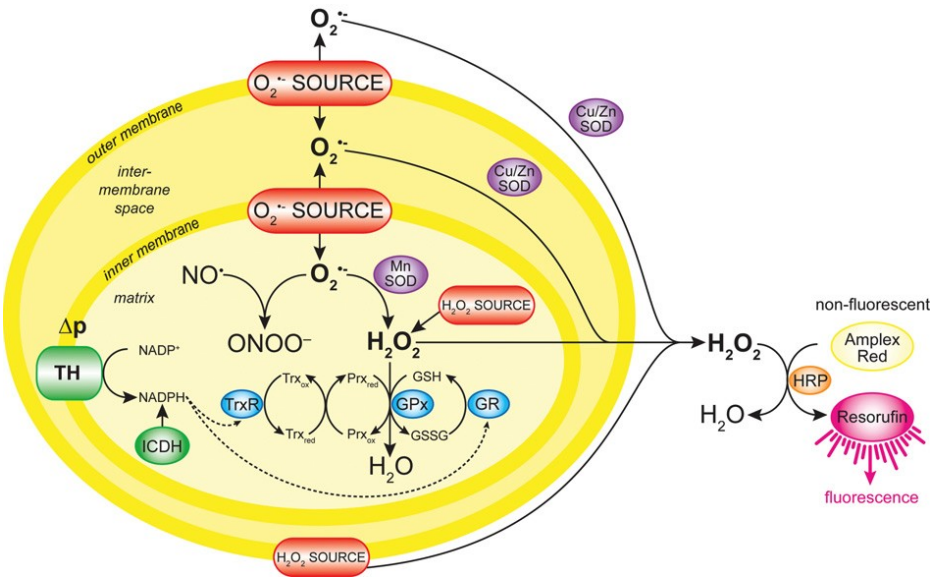

Figure 5: Overview of H_2O_2 Production in Mitochondria [27]

Not all H_2O_2 created by the mitochondria leaves the organelle; some is reduced to H_2O through interaction with glutathione peroxidases or peroxiredoxins [27]. Much of the H_2O_2 that leaves the organelle is converted into OH^- radicals through the Fenton reaction [29] through Fe or Cu reactants. These OH^- radicals, which in excess quantities along with other ROS, are components in oxidative stress. Oxidative stress is thought to be attributed as a primary cause of many ageing processes and disorders due to the damage caused to lipids and proteins [22][28][30].

2.7 Review of Related Research

While research has been conducted on the role of oxidizing elements in cellular healing [7][28][31] of arterial tissue, there is little focus on the effects oxidation has on the material response of that tissue. There have been only a few papers focusing on the subject to date [22][23], along with other research on the general response of elastin[20].

Stephen et. al, in our laboratory, published several papers on arterial tissue and the change in mechanical response of that tissue to varying treatments. For the focus of this thesis, one particular study stands out due to its focus on oxidation. In that paper, porcine aortas were obtained, cleaned of extra connective tissue, and cut into a total of 40 dog-bone specimens (10x30mm overall area, 5x7mm gage area) for treatment. Of those specimens, they were divided evenly into 5 different treatment groups. Additionally, 6 more specimens were treated using Lu's CnBR elastin isolation technique [2] and divided evenly to two different groups. Of the 5 groups of complete artery and 2 groups of elastin, 4 of the complete artery and 1 of the elastin groups were exposed to an oxidation solution of $FeCl_3$ [22]. The intact groups were treated for either 2, 4, 8, and 24 hours and the

elastin group was treated for 2 hours. Mechanical testing of the specimens was conducted to examine the uniaxial response of the specimens.

It was found that there was no significant difference between treatment groups for complete artery specimens when maximum stress and stretch ratio at maximum stress were examined [22]. The initial slope of the stress-stretch curve was noted to change as oxidation time increased. For isolated elastin, both the maximum stress and stretch ratio at maximum stress as well as the slope of the stress-stretch curve was found to change between treatment groups [22]. This shows evidence that oxidation has an effect on the material properties of arterial tissue, specifically on the elastin of the artery.

Gundiah et. al. [20] examined the basic mechanics of isolated elastin from porcine aortas through a more thorough mathematical approach than other sources. A generalized strain energy function was derived to a simplified form, reproduced in Equation 1, where c_0, c_1, c_2 are material constants and I_1, I_4, I_6 are invariants of the right Cauchy-Green Tensor.

Equation 1: $$W = c_0(I_1 - 3) + c_1(I_4 - 1)^2 + c_2(I_6 - 1)^2$$ [20]

The samples were tested biaxially instead of uniaxially using a pair of uniaxial arms operating at right angles to each other. A total of 6 samples

were obtained and the elastin was isolated using the autoclaving method described in section 2.5. The samples were cut to a sample size of 25.4mm square, although the paper does not indicate if this measurement was done before or after isolation. Marker beads were applied to the surface of each sample to measure surface displacement and a set of 4 load cells were incorporated along the axes. It was found that elastin, when examined using the strain energy function detailed in the paper, showed an elastic modulus of approximately 0.5MPa [20].

Ballinger et. al. [31] examined the effect of H_2O_2-sourced oxidation on the function and DNA integrity of mitochondria. This was approached through treating endothelial cells and smooth muscle cell cultures with O_2^-, H_2O_2, or $ONOO^-$. Treatment concentrations for H_2O_2 ranged from 50 to 200 μmol/liter to approach quantities found in the body. These treated cultures were then examined using DNA isolation and Quantitative Polymerase Chain Reaction analysis procedures to determine the amount of damage caused. It was found that exposure to reactive species caused mitochondrial DNA damage in both types of cells [31]. Exposure to reactive species was also determined to cause a reduction in mitochondrial function and ultimately concluded to be a possible factor in chronic vascular disease [31].

While the focus of Ballinger's work relates to cellular function and not protein composition, the conclusion that exposure to oxidizing agents, even in small concentrations, shows a wider-reaching effect on arterial tissue.

Examination of how oxidative stress caused by H_2O_2 and other reactive species interacts with the healing response and incidence of atherosclerosis was also performed by Rojkind et. al. [28] as well as Stocker and Keaney [7]. Rojkind's work covers a review of ROS production and reduction and how these oxidants play a part in the progression of aging-related disease and disorders. Most relevant to this work is a review of cellular sources of H_2O_2, which is incorporated in the discussion of hydrogen peroxide in Section 2.6. Stocker's work focuses on review of oxidative stress in artery walls and its relationship with atherosclerosis. The conclusions obtained through the review is that while there is evidence linking oxidation to atherosclerosis, exactly how those two points are linked is not clear [7].

Examining each of these papers shows several conclusions that can be applied toward the focus of this research. First, the material properties of structural arterial tissue can be evaluated through modified traditional engineering techniques and that there are several well-established methods to do so. Second, the effect that oxidizing elements, such as H_2O_2, have on

tissue has been explored, but primarily from a cellular perspective and not a mechanical one. And finally, H_2O_2 is an oxidizing agent commonly found naturally in the body as well as introduced during medical procedures, making it a relevant focus for experimental research. Therefore, it is the purpose of this research to apply these conclusions to form an analysis of the effect H_2O_2 has on arterial elastin to begin constructing an applicable model of the role oxidation has on arterial tissue mechanical behaviour.

3.0 Methods

3.1 Equipment

The Biological Material Testing System (BiMaTS) is a mechanical testing system used in this research to test the material properties of low-stress materials, specifically biological samples [32]. Much of the assembly is shown in Figure 6 and is comprised of 3 mechanical sub-assemblies with a supporting software program written in LabView.

The first assembly, seen in Figure 8, is the stepper motor and rail table. A 30V controller with a stepper motor (Applied Motion Products Inc., Watonsville, CA) moves the stage assembly. Displacement of the stage is measured by an optical encoder located on the side of the stage.

The second assembly is the specimen stage and environmental chamber, shown in Figure 7. This assembly has three major parts, the upper and lower specimen grips, the rail table, and the specimen chamber. The grip section uses a simple screw fixture to hold specimens between two pieces of textured plastic on each grip, shown in Figure 9. The upper grip is fixed to a load cell (Honeywell, Columbus,

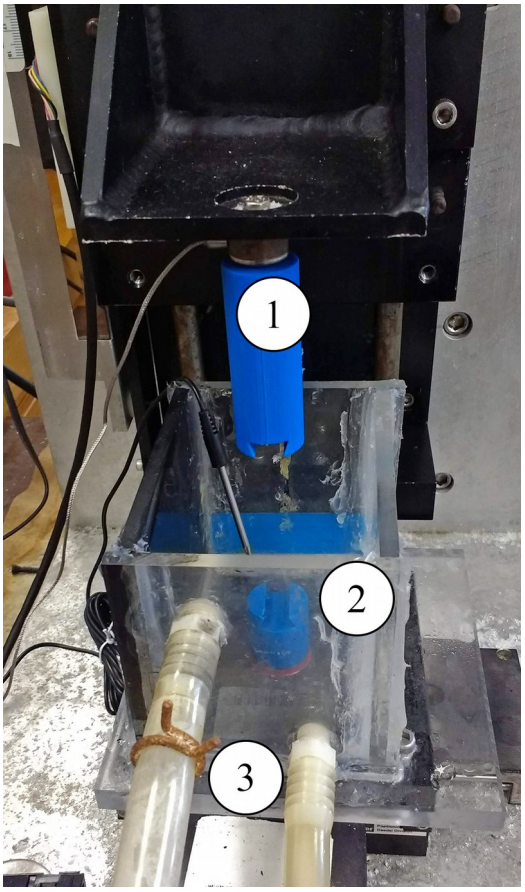

Figure 7: BiMaTS Specimen Chamber Assembly; 1) Upper Grip Attachment and Load Cell, 2) Lower Grip Attachment in Specimen Tub, 3) Inlet and Outlet to Pump and Heater Tub

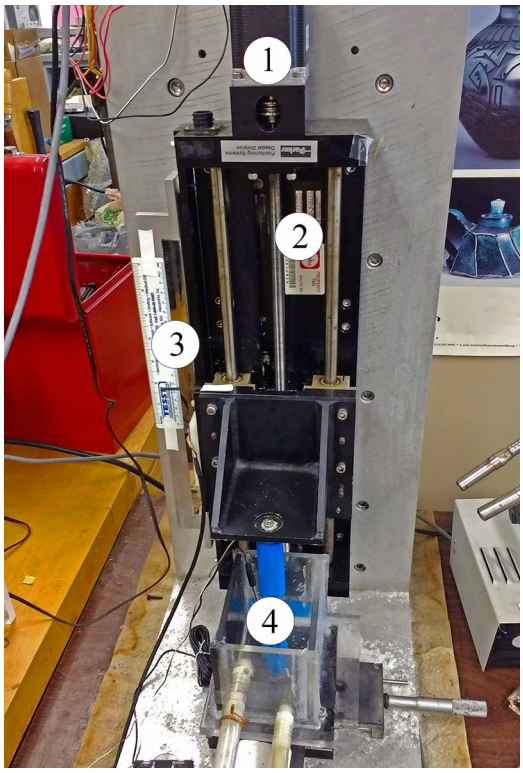

Figure 6: BiMaTS Loadframe Assembly; 1) Stepper Motor, 2) Rail Table, 3) Optical Encoder, 4) Specimen Tub

OH), which has a maximum load of 2.27kg (5lbs), which is in turn fixed to the stage moved by the motor assembly. The lower grip is attached to the bottom of the chamber. A pump assembly is connected to the specimen chamber to immerse specimens in saline solution, which is circulated and heated to simulate a more accurate in vivo temperature and environment for the in vitro testing system.

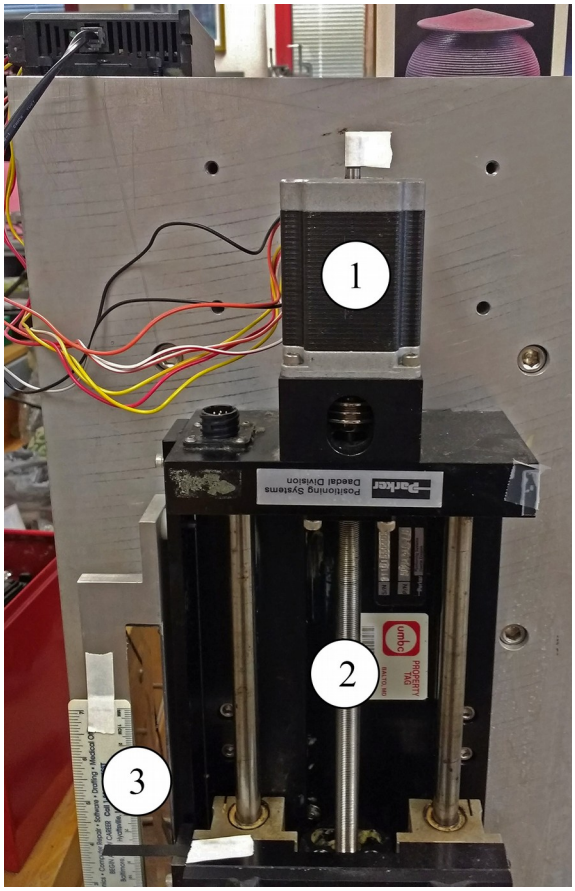

Figure 8: BiMaTS Stepper Motor and Rail Table; 1) Stepper Motor, 2) Rail Table, 3) Optical Encoder

The final component assembly is the pump and heater tub, shown in Figure 10. The pump circulates the saline solution between the specimen chamber and heater to evenly heat the solution and regulate the desired temperature. Heating is accomplished using a heating element suspended in the tub. Control of the heater is achieved through a digital thermometer placed in the

specimen chamber and a manual control loop to disconnect the heater once the solution has reached the desired temperature. Recorded specimen tub temperatures were in the range of 37.5±1.5 °C.

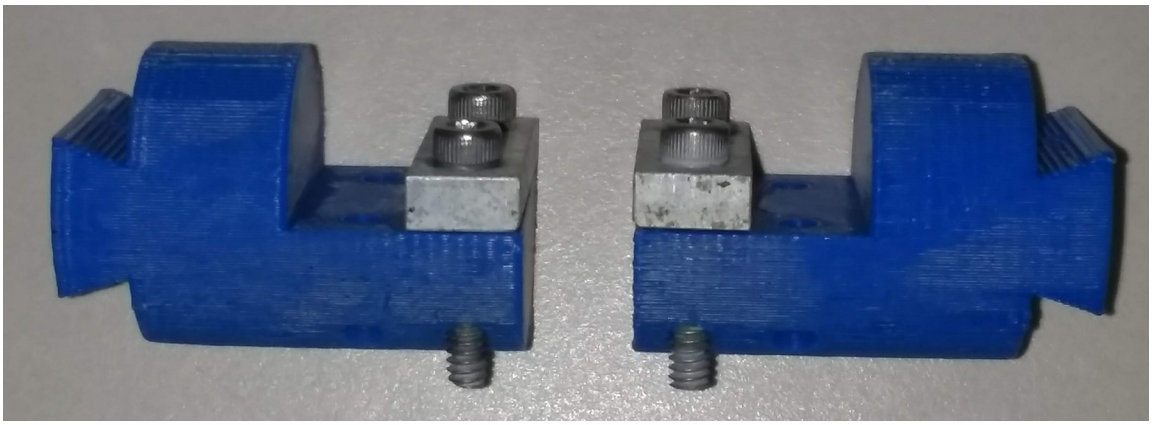

Figure 9: BiMaTS Specimen Grips

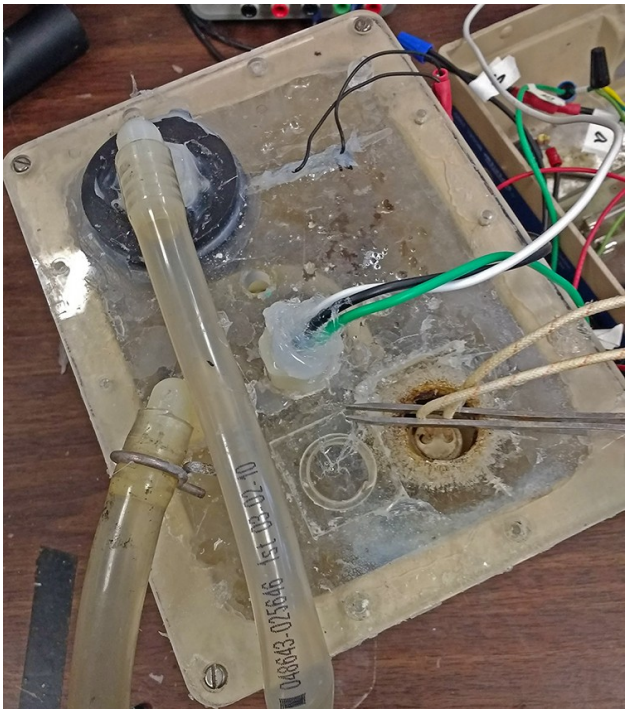

Figure 10: BiMaTS Pump and Heater Tub

The operation of the BiMaTS hardware is controlled through a custom-written Labview program. It is capable of operating the stage in both monotonic loading, where the stage moves at a constant speed to a designated distance from its starting location, and two modes of testing fatigue: one to a specified maximum force and another to a specified maximum position. For this experiment, only the monotonic mode was used. The Labview program was also designed to read both the load cell and optical encoder displacement data and record their force and position outputs in a Test Data Management System (.tdms) file.

3.2 Materials

Porcine Aortas were sourced from a local butcher (Wagner Meats LLC, Mount Airy, MD) from 6-month-old pigs and transported by cooler as received to the lab for preparation. A total of four aortas were obtained, three of which are shown in Figure 11. Once in the lab, they were cleaned of any excess tissue and cut along the longitudinal axis, as shown in Figure 12 with the longitudinal axis shown in purple. These samples were cut into dogbone specimens (5mm x 21mm, gage section 9mm x 3mm) so that the testing axis was aligned with the hoop axis, following the dogbone schematic on Figure

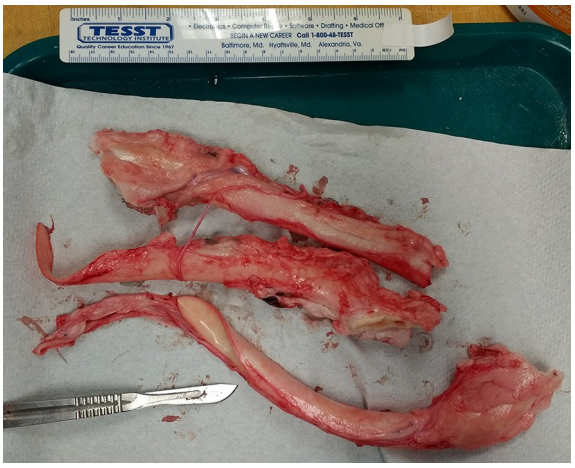

Figure 11: Uncleaned Pig Aortas

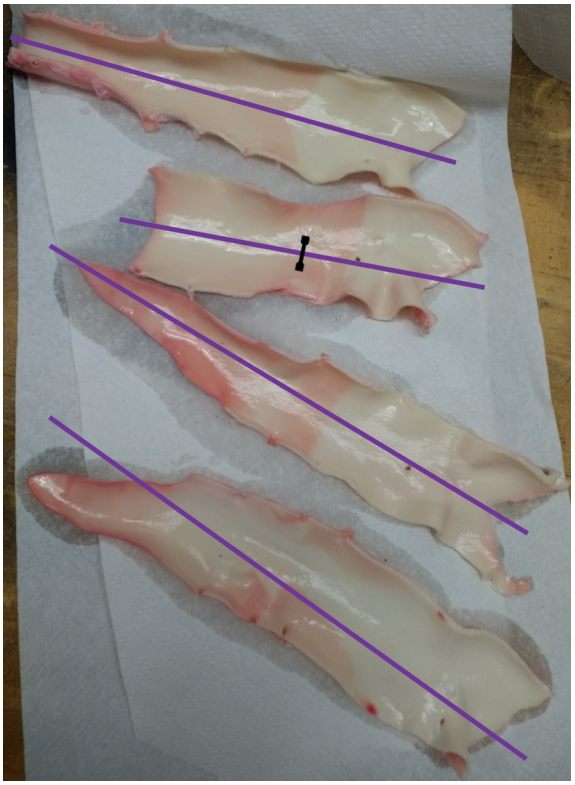
Figure 12: Cleaned and Opened Pig Aortas; purple lines indicate longitudinal axis, black dog-bone indicates approximate sample size and cutting orientation

12. Dr.s Stephen and Washington [22][23] had previously made a custom-made dogbone specimen punch, shown in Figure 13, which was used to create the total of 50 samples for testing. The samples were treated to isolate the elastin as described in Section 3.3 as a single group. During the sample cutting process, the arteries were rinsed with deionized water to keep them moist. While using Dulbecco's Phosphate Buffered Saline (DPBS; Thermo Scientific, Rockford IL) would have been preferred, the laboratory had a limited stock at the time and it was conserved for later

steps in the experiment instead of delaying this portion of the experiment and waiting for more to be delivered.

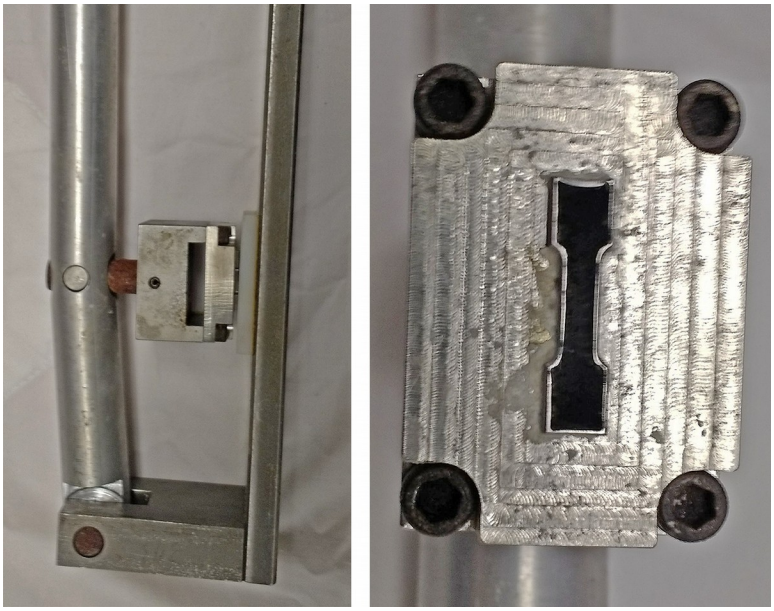

Figure 13: a) Specimen Punch b) Specimen Punch Die Side View

3.3 Elastin Isolation Procedure

The elastin scaffold isolation procedure followed that was previously used in the lab [22][23] and was obtained from Lu et. al [2]. Briefly, the samples were rinsed in DPBS and placed in a 50 mg/ml CNBr in 70% Formic Acid solution. The samples were gently stirred at room temperature (20-24 °C) for 19 hours. The samples and treatment solution were then heated to 60 °C for 1 hour, then heated to 100 °C for 5 minutes to inactivate the CNBr while continued to be stirred gently. The samples were removed

from the solution and rinsed with DPBS. The samples were stored idle in DPBS at 5 °C for three days before further processing.

3.4 H_2O_2 Treatment Procedure

The isolated elastin samples were separated into 10 groups, with 5 samples per group, for H_2O_2 oxidation treatment. The stirring that occurred during the elastin isolation treatment was determined to be a sufficient method of mixing and randomization, so they were placed in groups (5 samples to group 0, then 5 to group 1, etc.) directly from the CNBr solution using a pair of forceps. One group was left unoxidised as a control and as a reference to existing data and is referred as Group 0. The other specimen groups were submerged in enough 3% H_2O_2 and 97% distilled water solution (Rite Aid brand 3% Hydrogen Peroxide Topical Solution) to cover the samples completely for different exposure times as indicated by Table 1. Once the H_2O_2 treatment was finished for a particular group, that group's samples were rinsed in DPBS and stored in DPBS at 5°C until mechanical testing the next day.

Table 1: Sample groups and H2O2 Treatment Time Matrix

Sample Group	H_2O_2 Treatment Time	Sample Group	H_2O_2 Treatment Time
0	No Treatment	5	2 hours
1	5 minutes	6	4 hours
2	15 minutes	7	8 hours
3	30 minutes	8	16 hours
4	60 minutes	9	24 hours

3.5 Sample Testing Procedure

The samples were tested on the BiMaTS in order of group, starting with Group 0. All tests were completed within two days. Prior to testing, the pump and heater reservoir was filled with fresh DPBS (~2L) and allowed to heat up to 37°C. The sample dimensions were measured with digital calipers with care being taken to not to overly deform or damage the samples. The samples were then carefully placed in the grips, tightened in place, and gently loaded into the testing apparatus, as shown in Figure 14. Manual control was used to remove slack in the sample, with careful observation of the load cell readout to prevent applying a pre-load greater than 5 grams. A monotonic tension test was then run via the software control until the

specimen failed. Once failure occurred, the test was stopped, the broken sample removed, and the process was repeated with the next sample.

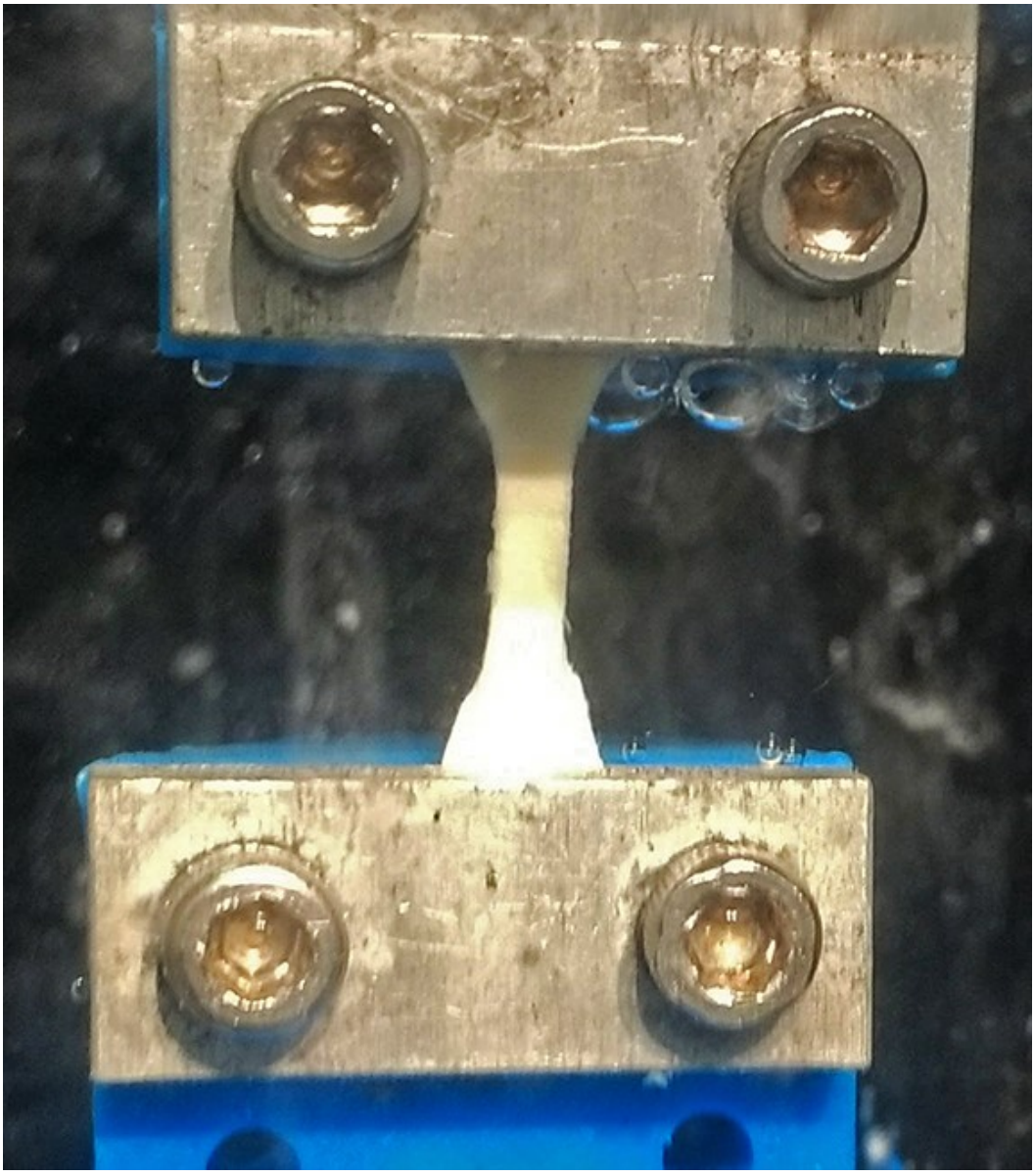

Figure 14: Specimen in Grip

3.6 Data Processing

After all of the load-deflection data were collected, the .tdms files were converted into .ods (Open Document Spreadsheet) files and processed using LibreOffice. Each sample group's data were collected into a single spreadsheet for ease of viewing. The force and displacement data were used to calculate stress and stretch using the engineering stress and stretch ratio equations:

Equation 2: a) $\sigma = F/A$

b) $\lambda = l/l_0$

where σ – Stress (MPa), λ – Stretch Ratio (mm/mm), F – Force (N), A – Initial Cross-sectional Area (m^2), l – Current Length (mm), and l_0 – Initial Length (mm).

The stress/stretch data were graphed and the maximum stress values were determined using the MAX function. The stretch at the maximum stress was found using the MATCH and ADDRESS functions and these data points were collected into a single spreadsheet document to make later calculations easier to perform.

Some samples showed additional signal distortion in the graphs that exceeded the background noise of the BiMaTs itself. To determine if the

distortion affected the maximum stress and stretch data, the following procedure was used. A region of excessive distortion was defined as a region where the difference between the peaks and valleys of nearby data points, referred to as the band width, are spread over a visually estimated 1.5x the band width of the majority of the data's estimated band width. An example of this is shown in Figure 15, where the line marked A is the start of the distortion region, and the line marked B is the end of the distortion region. This distortion region is considered to end once the band width is no longer over 1.5x the established normal width. Once this region is identified, if it exists at all for a sample, the location of the region on the graph is evaluated to determine how to proceed. If the highest peak of the region does not exceed the visually-obtained maximum stress, no action is taken, because the distortion does not affect the calculations used. If the region exceeds the visually-obtained maximum stress but is not occurring over the failure point of the sample, the cells referenced in the MAX function are modified to only include the region around the failure point. If the region occurs over the failure point of the sample, that sample was removed from further calculations. An example of an excluded sample is shown in Figure 16.

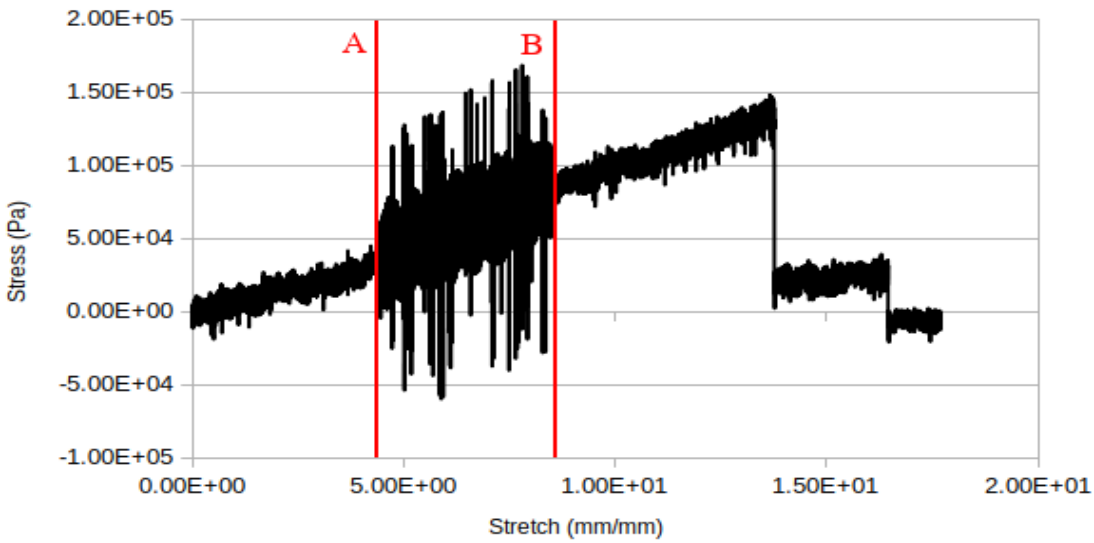

Figure 15: Group 0, Sample 3 - Significant Distortion Example; reference cell adjustment required

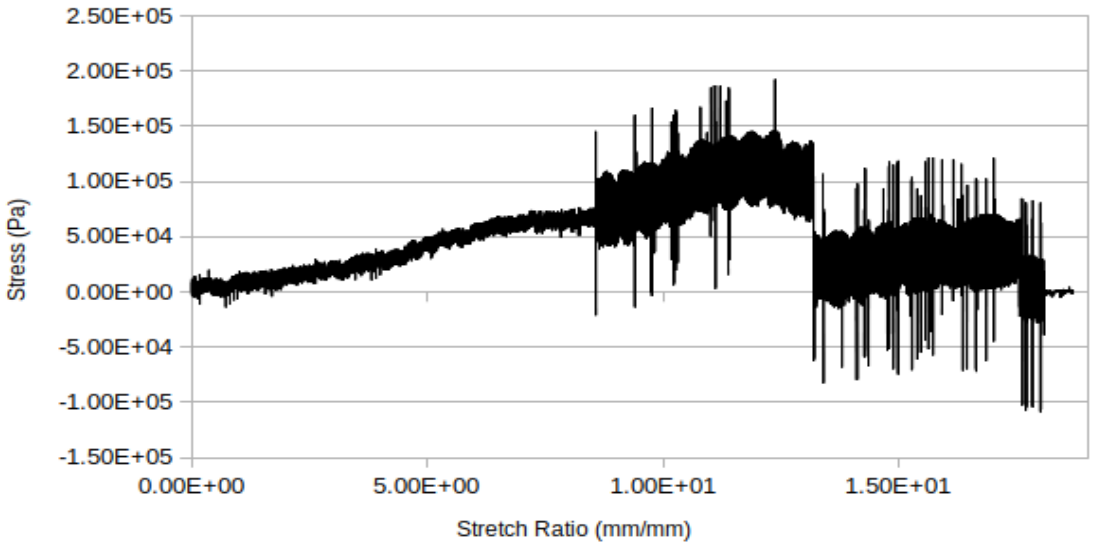

Figure 16: Group 3, Sample 5 Graph – Significant Distortion Example; meets data exclusion criteria

To identify any differences between the control group and treatment groups, two statistical methods were employed, one-way ANOVA with Tukey Honest Significant Difference (HSD) post-hoc analysis and Bland-Altman plots. The one-way ANOVA and Tukey HSD data were generated through the "aov" and "TukeyHSD" functions in R, respectively [33]. The complete list of commands used with detailed instructions are listed in Appendix B. The Bland-Altman plots [34] were created with LibreOffice Calc using the following equations:

Equation 3: a) $$x_n = \frac{(Gr_{0avg} + Gr_n(m))}{2}$$

b) $$y_n = Gr_{0avg} - Gr_n(m)$$

where x_n is the x-axis for Group n, y_n is the y-axis for Group n, Gr_{0avg} is the average value for Group 0, and $Gr_n(m)$ is the value for Group n, Sample m.

As part of the comparison criteria for a Bland-Altman plot, two lines at $\pm$1.96*Standard Deviation were plotted to indicate data points that deviate significantly from the control group's average. Equations 3a and 3b are applicable for both the Maximum Stress and Stretch at Maximum Stress Bland-Altman plots. A Bland-Altman plot is used to compare multiple data sets, in this case each H_2O_2 treatment group, to each other while taking into account data sets which have large variances, such as medical diagnostic

data [34]. Data points that fall between the two 1.95*Standard Deviation lines are considered to be supporting the hypothesis that the two sets are producing equivalent results [34]. An example of this is shown in Figure 17. In this case samples 2 through 5 fall within the two 1.95*Standard Deviation lines and thus support the hypothesis, and sample 1 falls outside that band and doesn't support the hypothesis.

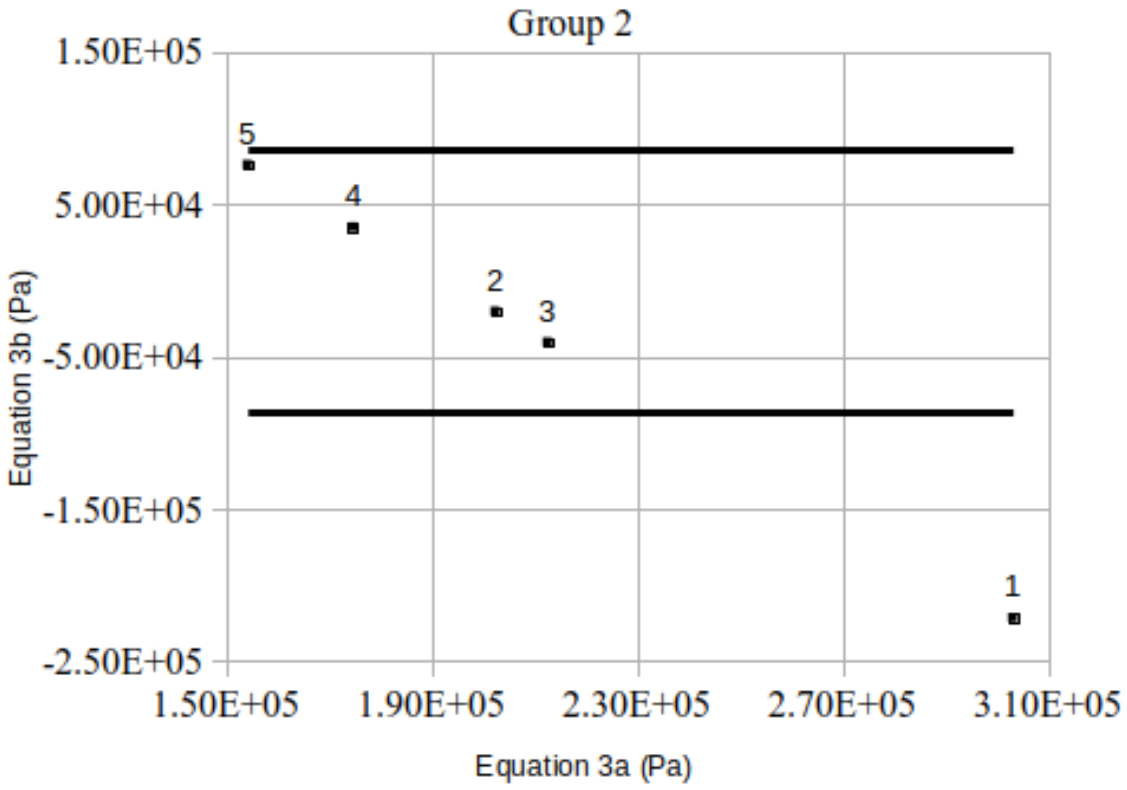

Figure 17: Bland-Altman Plot, Group 2

3.7 Predicted Results

The hypothesis that we were testing was that the tissue's mechanical response depends on the time of H_2O_2 exposure, which implies the extent of tissue oxidation by H_2O_2. This would lead to a measurable change in material properties as indicated by the maximum stress and stretch at max stress following a logarithmic curve, with one possible variation of this being illustrated in Figure 18. The increase in value as H_2O_2 exposure time increases was hypothesized as the most likely trend from observations gained through initial research [22][23][35].

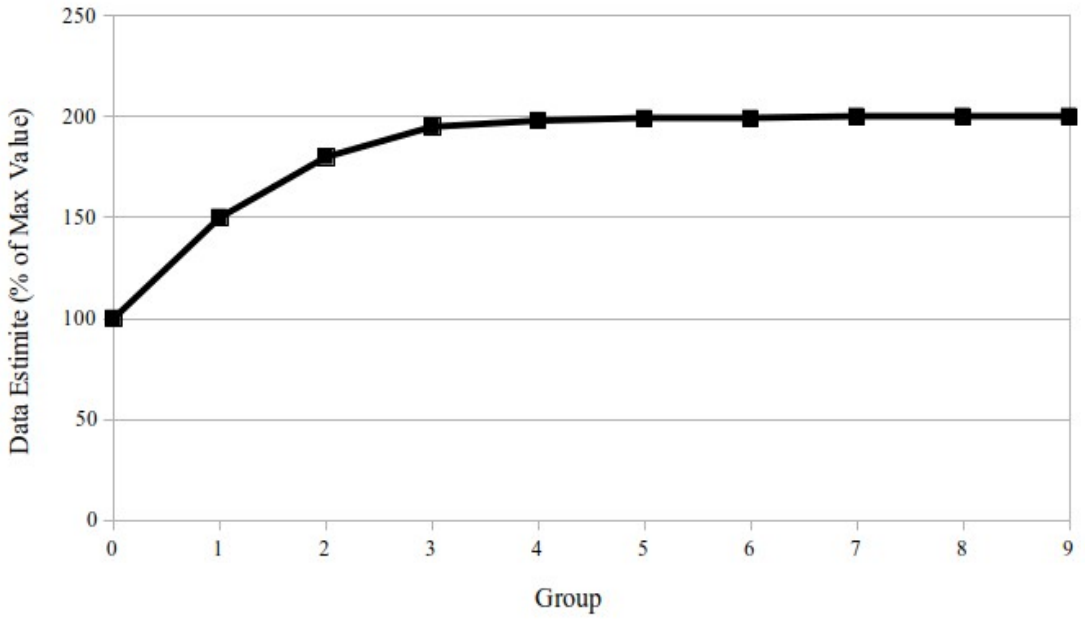

Figure 18: Elastin Response Estimate

4.0 Results & Discussion

4.1 Experimental Results

Once the experimental data were fully processed, the Maximum Stress and Stretch at Maximum Stress graphs did not show the expected response as described in section 3.7. The Average Maximum Stress and Strain at Max. Stress graphs are shown in Figures 19 and 20, and show very little change between each group as the treatment time increased. The numeric table data for these graphs is shown in Appendix A.

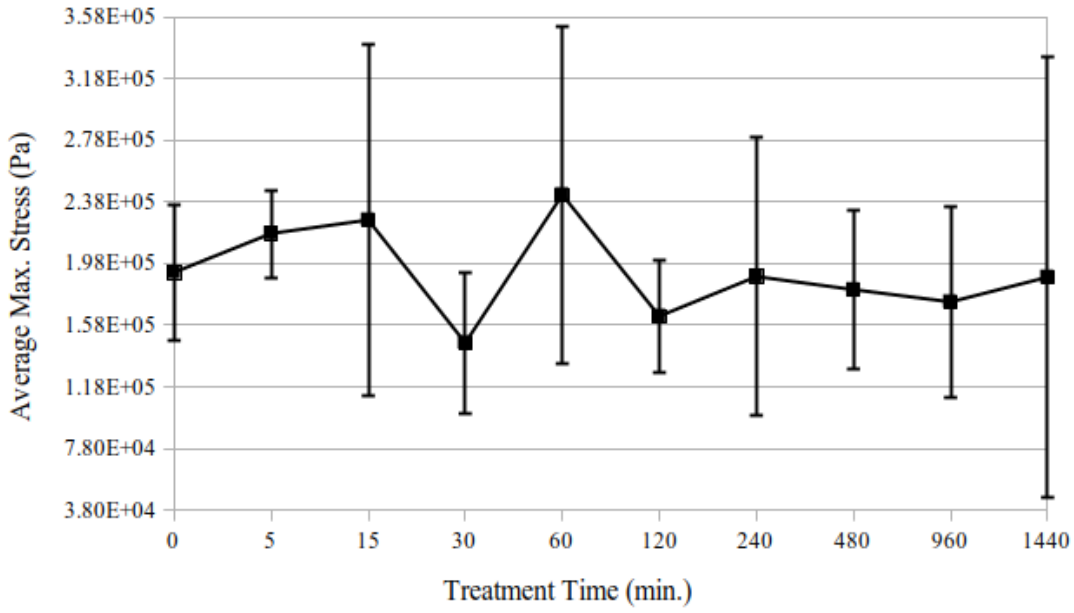

Figure 19: Average Maximum Stress by treatment group with error bars of one standard deviation indicated

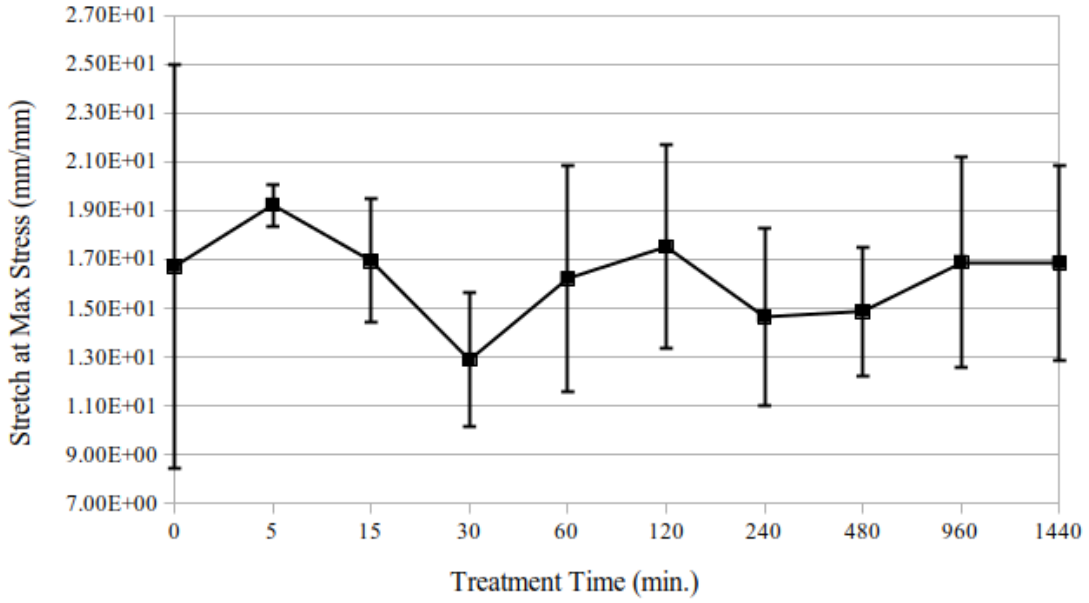

Figure 20: Average Stretch at Maximum Stress by treatment group with error bars of one standard deviation indicated

4.2 Data Analysis

The ANOVA data for both the Max. Stress and Stretch at Max. Stress is detailed in Tables 2 and 3 respectively. A summary of the Tukey HSD results showing notable group comparisons is shown in Table 4, with the full set of pairs shown in Appendix A. The data show a confirmation of the initial observation that the data has no significant change in properties as treatment time increased, indicated by high p-values (>>0.05). The lowest p values for Max. Stress was group pairing 9-3 with an adjusted p-value of 0.55 and for Stretch at Max. Stress was group pairing 3-1 with an adjusted p-value of 0.46. All other p-values for the Tukey HSD are greater than those

listed, further supporting the ANOVA results that there is no significant difference between treatment times.

Table 2: One-way ANOVA Output for Stress Data

	Df	Sum Sq	Mean Sq	F value	Pr(>F)
Group	9	4.261e+10	4.734e+09	0.976	0.477
Residuals	34	1.649e+11	4.851e+09		

Table 3: One-Way ANOVA Output for Stretch Data

	Df	Sum Sq	Mean Sq	F value	Pr(>F)
Group	9	124.7	13.85	0.762	0.651
Residuals	34	617.8	18.17		

The construction of Bland-Altman plots for each group compared to the Group 0 average provides an additional means of analysis. The plots are shown in Figures 21 and 22 for Max. Stress and Stretch at Max. Stress respectively, where the y-axis on each sub-plot is Equation 2b and the x-axis on each sub-plot is Equation 2a. The units for both axes for Figure 21 is in Pa, and mm/mm for Figure 22. In the case of this experiment, the hypothesis tested using the Bland-Altman plots is that there is no change in Maximum Stress and Stretch at Maximum Stress from increased exposure to H_2O_2.

Table 4: Notable Tukey HSD Data

Stress Data	diff	lwr	upr	p adj
Group9-Group3	1.02e+5	-6.46e+4	2.68e+4	0.5595
Group9-Group5	8.45e+4	-7.34e+4	2.43e+5	0.725
Stretch Data	diff	lwr	upr	p adj
Group3-Group1	-6.36e+0	-1.60e+1	3.310e+0	0.461
Group6-Group1	-4.595e+0	-1.37e+1	4.52e+0	0.785

The Bland-Altman plots for Stress weakly support the hypothesis with 74% (29/39) of the data points within the boundary conditions. 100% (39/39) of the Stretch data points are contained within the 95% limits of agreement boundary conditions, fully meeting the criteria detailed for Bland-Altman plots.[34] These plots show that each treated data point, excluding the 10 data points in the Stress data, were within the 95% limits of agreement for the untreated average. These results further support the initial observation and ANOVA data that there is no significant difference between treatment times of H_2O_2 on the uniaxial tensile response of arterial elastin.

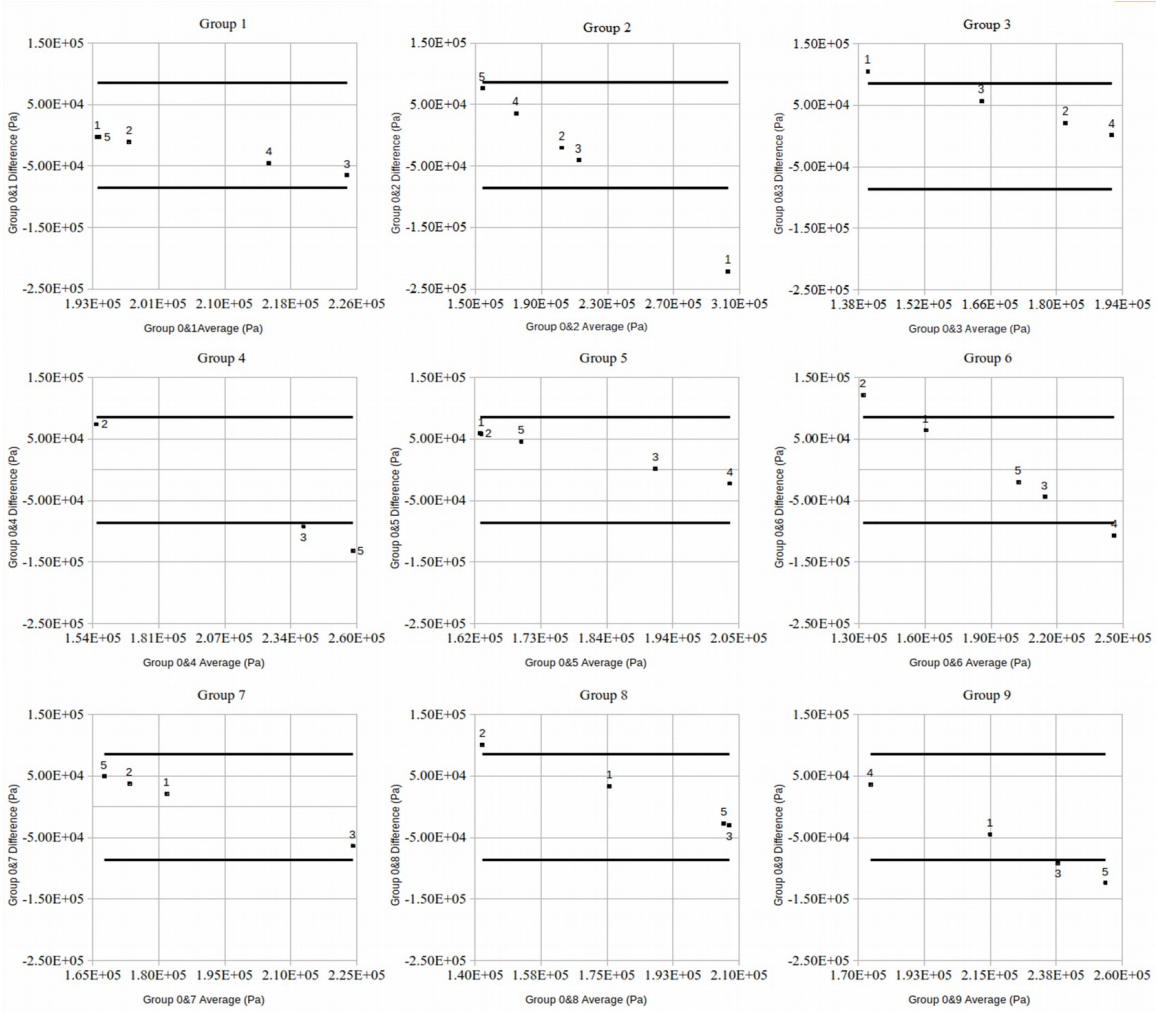

Figure 21: Bland-Altman Plot for Stress

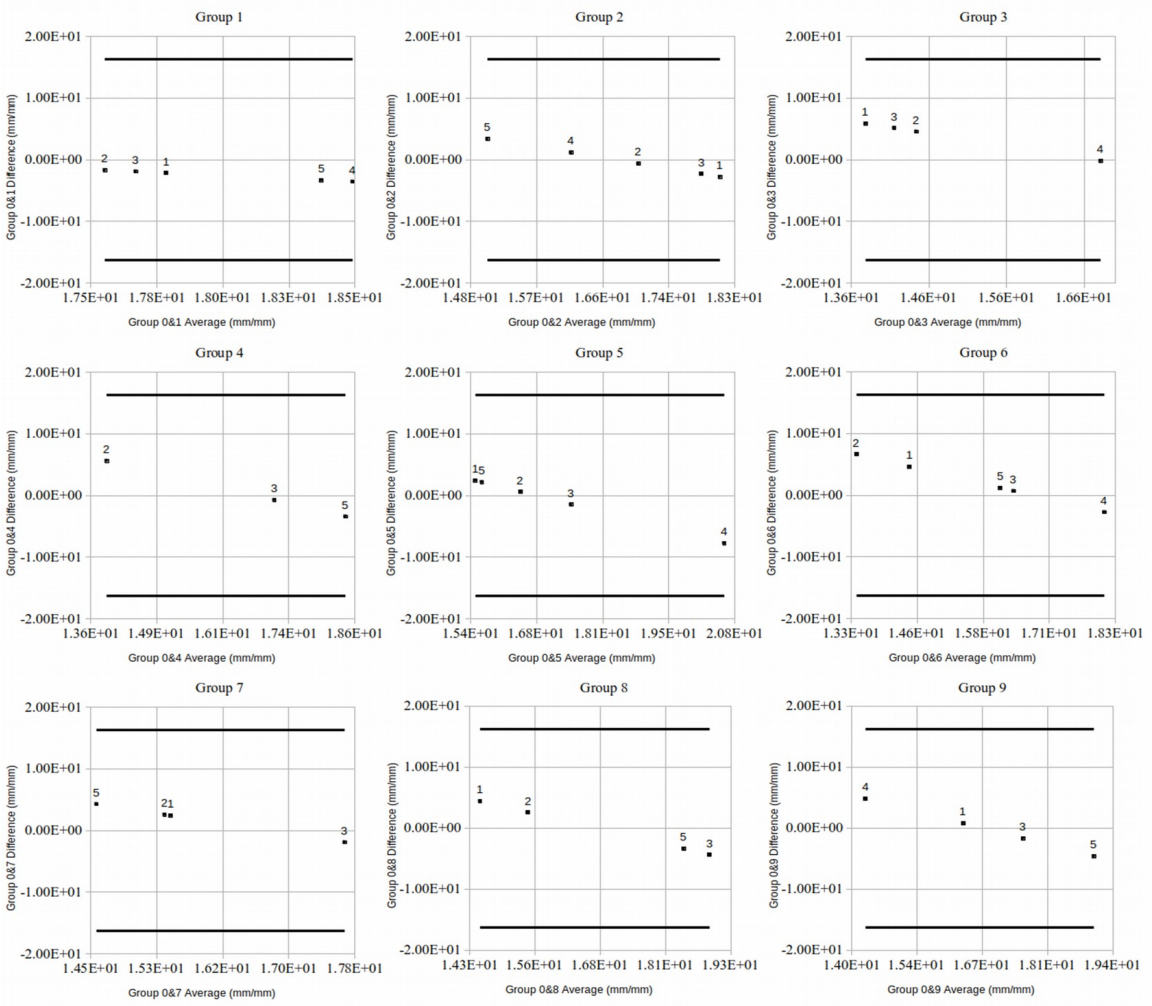

Figure 22: Bland-Altman Plots for Stretch

4.3 Discussion

These results can be examined in further depth to evaluate the effect of H_2O_2 on elastin. As previously described (Section 2.6), H_2O_2 is a commonly found oxidant that appears in cellular processes and is also used as a chemical in medical applications. Section 2.7 discussed how other

authors have approached topics related to this experiment. There were several observations of interest in the experimental data, the persistent noise throughout the data, the intermittent distortion, and the large standard deviations.

4.3.1 Noise and Distortion Identification

As part of the process to identify the source of the noise and distortion, two additional sets of tests were conducted. One set of three tests were done with no sample, and are referred to as the calibration tests, one of which is shown in Figure 23. The other set of tests were conducted with a rectangular length of elastic band cut to approximately 40mm in length, and

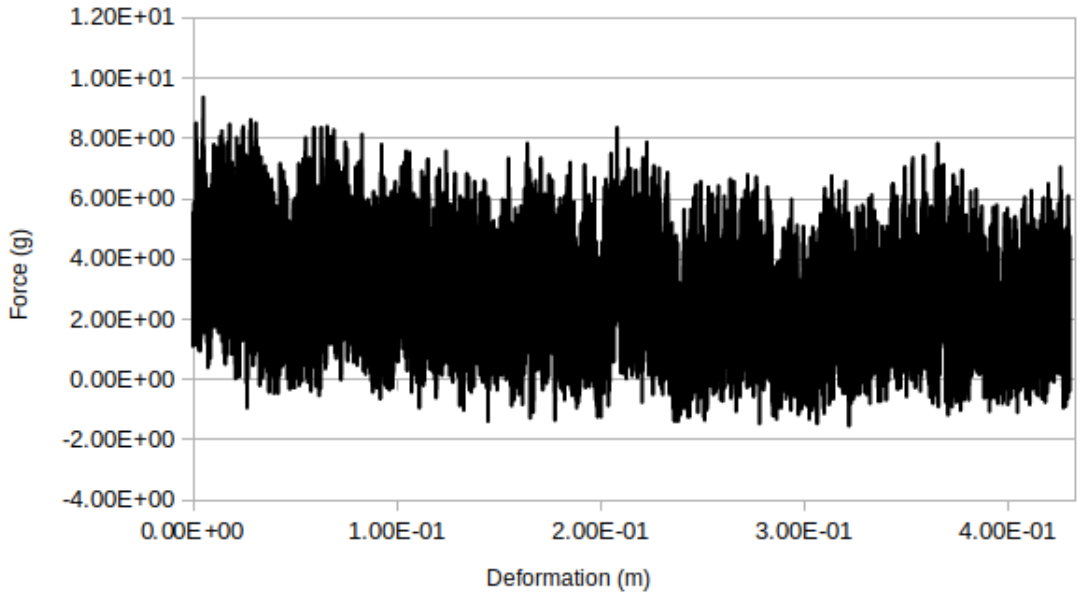

Figure 23: Calibration Test Data

are referred to as the elastic tests, one of which is shown in Figure 24. Force and deformation is shown instead of Stress and Stretch as the calibration tests had no dimensions to measure and the elastic tests had no clear gage section to evaluate.

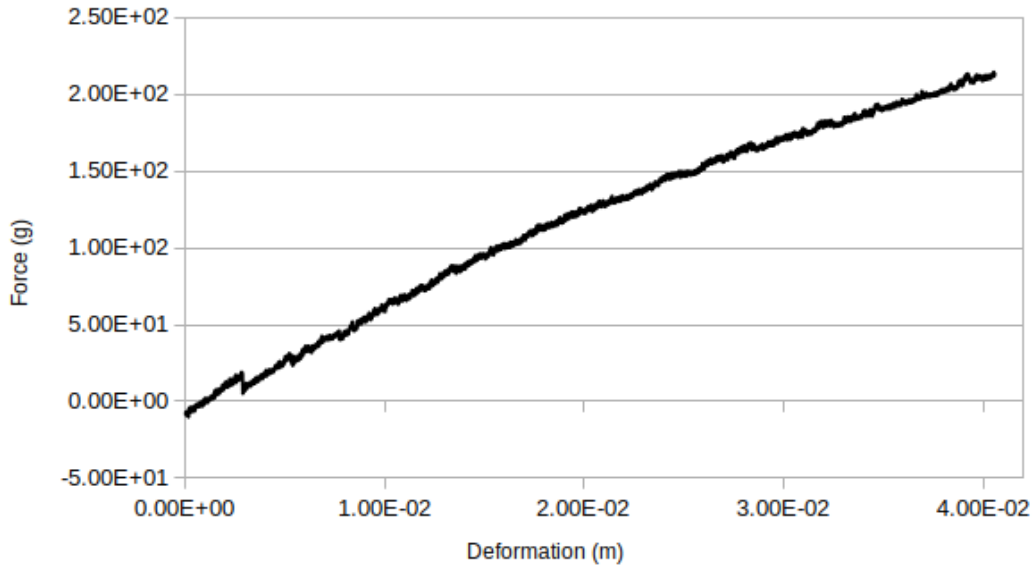

Figure 24: Elastic Test Data

4.3.2 Background Noise

The background noise was noticed in every single sample, including the calibration and elastic tests. Small subsets of each sample were calculated to compare the band width of the noise to try and determine if it is consistent across all samples. An evaluation of the range of values between the 15th and 45th data points found an average band width of 8.02 grams with

a standard deviation of 1.3 grams. This indicates that there is low variance in the noise across all groups, supporting that the noise is consistent and persistent throughout all data. These values exclude any samples which exhibited distortion over the evaluation region, but do include samples that were excluded from statistical analysis for distortion over the failure point. As a comparison, the elastic band tests had an average band width of 6.82 grams and the calibration tests have an average band width of 3.79 grams. The narrow number of samples cover a deformation of 3E-4 m near the start of the test and was chosen to try to avoid the change in force from the sample deformation overshadowing the background noise while still being able to capture an oscillatory response. Even so, the increased values for the experimental and elastic test band widths are including the increased load from the deformation.

Overall, the noise is a consistent element of the gathered data, and several sources for it have been examined. The age of the load cell could be a factor, as the testing apparatus had been left standing and unmaintained for at least a year. Electrical interference from the connections in the system itself could also cause the noise. Variation inherent in the load cell is a factor in the noise, with the load cell datasheet reporting data variation of up to

0.15% of the full scale, a peak of 3.4 grams for the particular load cell used in BiMaTS [36]. An additional cause of the noise would be vibration caused by the stage motion or air currents interfering with the load cell readout. Sensor variation and vibration from the stage moving seems the most likely causes of the passive background noise seen in Figure 25, as the BiMaTS is not on a vibration-absorbing bench and the load cell side of the specimen grip is open to the air as can be noticed in Figure 7. The peak variation provided in the data sheet is within the values gathered for the calibration test, and vibration from the stage operation is the most logical source for the remainder of the noise.

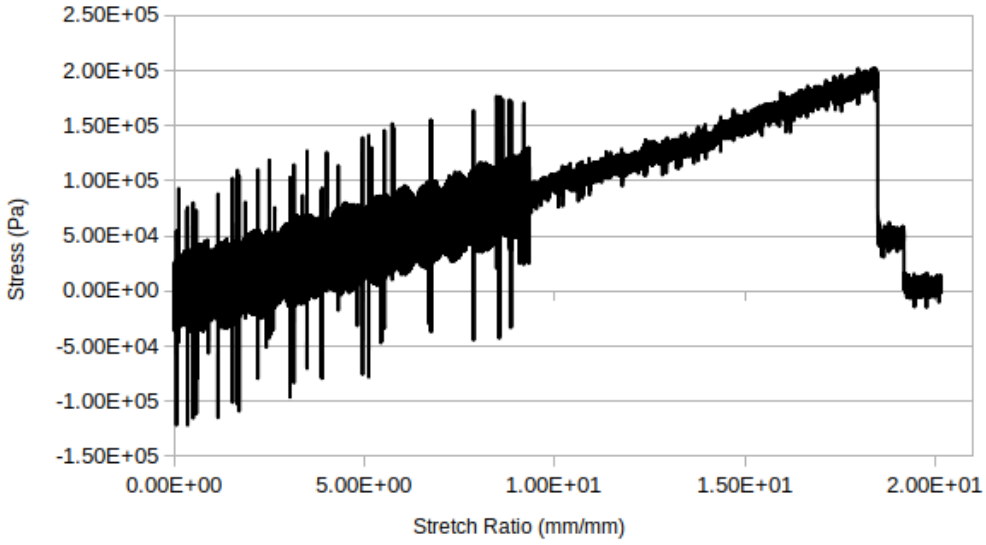

Figure 25: Group 1, Sample 2 Stress/Stretch Graph

4.3.3 Intermittent Distortion

Finding the source of the observed distortion proved to be less decisive. Neither the calibration nor the elastic tests exhibited the intermittent distortion that was observed in the experimental data. Because the distortion wasn't reproducible, it is concluded that the problem occurred with the samples themselves and how they were fixed and loaded into the testing system instead of an inherent problem with the BiMaTS. Electrical interference is the only cause of those listed in section 4.3.2 as possibly contributing to the distortion.

Because the distortion didn't occur during later controlled testing and the procedures for the experimental data didn't account for examination for distortion in the data during the primary experiment, no clear conclusion can be made on where the distortion comes from. Regardless of the source of the distortion, it was observed that the recorded maximum values for each sample are those seen on the peak of the graph and not from a sudden spike earlier in the experiment using the selection criteria described in the Methods section. A total of 6 samples across five different groups met the criteria where the region of elevated noise occurred directly near the failure point, making that data unusable.

4.3.4 Data Variance

An additional observation of interest was that once all the sample data for each group were collected and analysed, there was noticeable variation in the average stress and stretch values within a group, with the standard deviations for Max. Stress ranging from 2.84E4 (13% of the average value for that group) to 1.43E5 (76%) Pa and standard deviations for Stretch at Max. Stress ranging from 8.55E-1 (4%) to 8.29E0 (50%) mm/mm.

This large standard deviation could have been initiated through several factors. First, the samples could have been over- or under-tightened in the specimen grips, as they are tightened by hand it would be very easy to have this accidentally occur. Second, the samples could have been cut slightly misaligned from the hoop direction, as only visual scale (ruler and observation) verification was used to ensure the samples were aligned. As discussed in section 2.5, arterial elastin is aligned biaxially through the axial and hoop directions, but does not have full isentropic fiber arrangements. By misaligning the samples, instead of the testing axis being aligned with one of the fiber axes, it is aligned with neither of them and produces a shear response, which would produce lower maximum stress values. Third, the composition of tissue in the artery changes as it proceeds further from the

heart [5], while the samples obtained were all from the aorta, the location from which they were obtained could cause some variation in composition. Fourth, the precise age of the pigs sourced for aortas was not obtained beyond the ballpark figure of 6 months. Subtle age-related factors could have caused some variation in data gathered. Finally, as the samples were isolated all in one group and the tissue composition was not verified, some samples could have had some residual tissue, producing a slightly different response.

4.3.5 Sample Physical Response

Even though video documentation of the samples was not obtained during testing, some samples were still able to be visually observed during material testing. As the samples deformed, it was observed that failure occurred in two stages, where one layer of the elastin failed before the other. This behaviour can be seen in the Stress/Stretch graphs, such as Figures 15, 16, and 25 where the stress drops in two separate stages. Due to the treatment processes conducted on the samples, it is unclear from observation which of the two major elastin sheets failed first, but from understanding of elastin fiber arrangements the Intimal layer would likely fail before the

Medial layer. This is because the Intima elastin layer is thinner and aligned perpendicular to the testing axis. Dr. Washington also noted this behaviour in the elastin samples during testing [23].

4.4 Data Comparison with Prior BiMaTS Research

While several different data analysis methods were applied, it is still valuable to compare the results of this research with other similar work, which in this case is the research of Dr.s Stephen and Washington. Dr. Stephen's work on oxidation [22] shows an increase in the maximum stress of the elastin oxidized by a 67 mM $FeCL_4$ and 0.02% NaN_3 solution from 0.12±0.05 MPa with no oxidation to 0.21±0.06 MPa with elastin oxidized for 2 hours. This compares to the Group 0 data of 0.18±0.05 MPa to the Group 5 average of 0.15±0.03 MPa covering the same 2 hour oxidation time. There is an 80% increase in the maximum stress in Dr. Stephen's results that is noted in her analysis [22] that is not reflected in the data gathered in this research. The stretch at maximum stress did not exhibit an observable change in Dr. Stephen's work [22].

In the case of Dr. Washington's work [23], there was no observed difference between untreated and oxidized elastin with respect to different

treatment groups using two-way ANOVA, however there was a difference found ($p<0.05$) between each fatigue cycle count. Comparing the mean and standard deviations, Dr. Washington found 0.249±0.037 MPa with no oxidation at 25k cycles to 0.265±0.030 MPa at 25k cycles with 2 hours of oxidation. This aligns with the trends obtained in this research, although the numerical values differ. Fatigue would produce different results as repeated cycles would magnify any existing specimen flaws or potentially change how the fibers are linked together, providing a reason for the differing values. That the overall trend of material response from monotonic loading in this work and from fatigue in Dr. Washington's work agree indicates that there is no evidence that oxidation has a statistically significant effect on the material properties of elastin.

4.5 Limitations

Several limitations were noted from the procedures followed for this experiment. First, it was noted that the final tissue composition of the samples was not determined, so it is not known exactly how pure the elastin samples were. Because elastin is insoluble, the most effective method of determining purity of an elastin sample is to determine whether there are

other amino acid components found in the sample and compare their total quantity to the entire sample [21]. Second, the tests were not video recorded nor photographed, except for Figure 14, so that any behaviour in the sample before failure could only be noted at the time of testing and not later reviewed for analysis. Third, the samples were isolated to elastin and then treated with H_2O_2, where as performing the H_2O_2 treatment then the elastin isolation could produce different results. Fourth, only monotonic tensile loading was performed, examining only the situation of a single instance of oxidative stress along with single large deformation as opposed to a long-duration intermittent exposure with a fatigue component. In addition, fatigue loading may magnify subtle material changes that are lost in the noise of the monotonic testing.

5.0 Conclusions and Future Work

While this research addressed the issues with evaluating the oxidation of elastin, the two primary source works also evaluated oxidation of untreated arteries as well as collagen. Further work would expand the experiments to evaluating H_2O_2 treatment of isolated collagen as well as untreated tissue. Furthermore, as the experiment done in this research was

only examining monotonic loading to failure, expanding the experiments to include fatigue would result in a closer approximation of in situ failure of arterial tissue due to material changes from oxidation. Oxidative stress occurs over the course of decades before it is detected [7], so a single instance of oxidation and testing is not a very accurate simulation of reality. Furthermore, the fracture surfaces and fracture behaviour were only observed with a naked eye during the testing. Adding more rigorous visual observation methods such as video recordings of the tests and high-powered microscopy of the fracture surfaces would increase the amount of data that can be gathered from the research, increasing the applicability of the results obtained.

6.0 Appendix

6.1 Appendix A: Experimental data tables

Red highlighted rows indicate data that was excluded from later calculations due to failing the exclusion criteria detailed in the Methods section. Unless otherwise indicated, columns referred to as Stress are in units of Pa, columns referred as Stretch are in units of mm/mm, and all other columns do not have units.

Table A1: Aggregated Data Averages by Group

Group	Average Max Stress	Median Max Stress	Stress Std. Dev	Average Stretch	Median Stretch	Stretch Std. Dev	Removed
0	1.92E+05	1.80E+05	4.38E+04	1.67E+01	1.44E+01	8.29E+00	0
1	2.18E+05	2.03E+05	2.84E+04	1.92E+01	1.89E+01	8.55E-01	0
2	2.26E+05	2.12E+05	1.14E+05	1.69E+01	1.73E+01	2.54E+00	0
3	1.46E+05	1.54E+05	4.54E+04	1.29E+01	1.19E+01	2.74E+00	1
4	2.43E+05	2.85E+05	1.09E+05	1.62E+01	1.74E+01	4.64E+00	2
5	1.64E+05	1.47E+05	3.68E+04	1.75E+01	1.61E+01	4.18E+00	0
6	1.90E+05	2.12E+05	9.02E+04	1.46E+01	1.55E+01	3.65E+00	0
7	1.81E+05	1.63E+05	5.12E+04	1.49E+01	1.42E+01	2.65E+00	1
8	1.73E+05	1.89E+05	6.18E+04	1.69E+01	1.71E+01	4.34E+00	1

Table A2: Group 0 Max Stress and Stretch Ratio Data

Sample #	Max Stress	Stretch at Max Stress
1	2.50E+05	2.90E+01
2	2.22E+05	2.07E+01
3	1.69E+05	7.79E+00
4	1.80E+05	1.17E+01
5	1.41E+05	1.44E+01

Table A3: Group 1 Max Stress and Stretch Ratio Data

Sample #	Max Stress	Stretch at Max Stress
1	1.95E+05	1.89E+01
2	2.03E+05	1.84E+01
3	2.57E+05	1.86E+01
4	2.38E+05	2.03E+01
5	1.95E+05	2.00E+01

Table A4: Group 2 Max Stress and Stretch Ratio Data

Sample #	Max Stress	Stretch at Max Stress
1	4.14E+05	1.95E+01
2	2.12E+05	1.73E+01
3	2.33E+05	1.90E+01
4	1.57E+05	1.55E+01
5	1.16E+05	1.33E+01

Table A5: Group 3 Max Stress and Stretch Ratio Data

Sample #	Max Stress	Stretch at Max Stress
1	8.76E+04	1.09E+01
2	1.71E+05	1.22E+01
3	1.36E+05	1.16E+01
4	1.91E+05	1.69E+01
5	1.92E+05	1.24E+01

Table A6: Group 4 Max Stress and Stretch Ratio Data

Sample #	Max Stress	Stretch at Max Stress
1	2.53E+05	1.52E+01
2	1.19E+05	1.11E+01
3	2.85E+05	1.74E+01
4	2.30E+05	1.39E+01
5	3.24E+05	2.01E+01

Table A7: Group 5 Max Stress and Stretch Ratio Data

Sample #	Max Stress	Stretch at Max Stress
1	1.34E+05	1.43E+01
2	1.33E+05	1.61E+01
3	1.90E+05	1.82E+01
4	2.15E+05	2.45E+01
5	1.47E+05	1.45E+01

Table A8: Group 6 Max Stress and Stretch Ratio Data

Sample #	Max Stress	Stretch at Max Stress
1	1.28E+05	1.21E+01
2	7.13E+04	1.01E+01
3	2.37E+05	1.60E+01
4	2.99E+05	1.95E+01
5	2.12E+05	1.55E+01

Table A9: Group 7 Max Stress and Stretch Ratio Data

Sample #	Max Stress	Stretch at Max Stress
1	1.71E+05	1.43E+01
2	1.54E+05	1.41E+01
3	2.56E+05	1.86E+01
4	3.54E+05	2.04E+01
5	1.43E+05	1.24E+01

Table A10: Group 8 Max Stress and Stretch Ratio Data

Sample #	Max Stress	Stretch at Max Stress
1	1.59E+05	1.23E+01
2	9.16E+04	1.41E+01
3	2.22E+05	2.11E+01
4	4.46E+05	2.28E+01
5	2.20E+05	2.01E+01

Table A11: Group 9 Max Stress and Stretch Ratio Data

Sample #	Max Stress	Stretch at Max Stress
1	6.97E+02	1.59E+01
2	3.22E+05	2.00E+01
3	2.84E+05	1.84E+01
4	1.56E+05	1.19E+01
5	3.16E+05	2.13E+01

Table A12: Tukey data for Stress

	diff	lwr	upr	p adj
Group1-Group0	25215.040	-123728.32	174158.40	0.9998709
Group2-Group0	34000.762	-114942.60	182944.12	0.9985719
Group3-Group0	-45851.317	-203829.61	112126.97	0.9914974
Group4-Group0	50333.909	-121651.07	222318.89	0.9909832
Group5-Group0	-28466.852	-177410.21	120476.51	0.9996511
Group6-Group0	-2717.625	-151660.99	146225.74	1.0000000
Group7-Group0	-11219.263	-169197.55	146759.03	0.9999999
Group8-Group0	-19197.893	-177176.19	138780.40	0.9999922
Group9-Group0	56075.048	-101903.24	214053.34	0.9673154
Group2-Group1	8785.722	-140157.64	157729.08	1.0000000

Group3-Group1	-71066.357	-229044.65	86911.94	0.8743042
Group4-Group1	25118.870	-146866.11	197103.85	0.9999625
Group5-Group1	-53681.892	-202625.25	95261.47	0.9640468
Group6-Group1	-27932.665	-176876.03	121010.70	0.9997008
Group7-Group1	-36434.302	-194412.59	121543.99	0.9984542
Group8-Group1	-44412.933	-202391.22	113565.36	0.9932239
Group9-Group1	30860.009	-127118.28	188838.30	0.9995838
Group3-Group2	-79852.079	-237830.37	78126.21	0.7828603
Group4-Group2	16333.147	-155651.83	188318.13	0.9999991
Group5-Group2	-62467.614	-211410.98	86475.75	0.9129561
Group6-Group2	-36718.387	-185661.75	112224.97	0.9974273
Group7-Group2	-45220.025	-203198.32	112758.27	0.9922936
Group8-Group2	-53198.655	-211176.95	104779.64	0.9766543
Group9-Group2	22074.286	-135904.01	180052.58	0.9999743
Group4-Group3	96185.226	-83680.97	276051.42	0.7257462
Group5-Group3	17384.465	-140593.83	175362.76	0.9999967
Group6-Group3	43133.692	-114844.60	201111.98	0.9945130
Group7-Group3	34632.055	-131891.69	201155.80	0.9993128
Group8-Group3	26653.424	-139870.32	193177.17	0.9999191
Group9-Group3	101926.365	-64597.38	268450.11	0.5595405
Group5-Group4	-78800.762	-250785.74	93184.22	0.8622483
Group6-Group4	-53051.534	-225036.51	118933.45	0.9870075
Group7-Group4	-61553.172	-241419.37	118313.03	0.9740894
Group8-Group4	-69531.802	-249398.00	110334.40	0.9451125
Group9-Group4	5741.139	-174125.06	185607.34	1.0000000
Group6-Group5	25749.227	-123194.13	174692.59	0.9998465
Group7-Group5	17247.590	-140730.70	175225.88	0.9999969
Group8-Group5	9268.959	-148709.33	167247.25	1.0000000

Group9-Group5	84541.901	-73436.39	242520.19	0.7249558
Group7-Group6	-8501.637	-166479.93	149476.65	1.0000000
Group8-Group6	-16480.268	-174458.56	141498.02	0.9999979
Group9-Group6	58792.673	-99185.62	216770.97	0.9562419
Group8-Group7	-7978.631	-174502.37	158545.11	1.0000000
Group9-Group7	67294.311	-99229.43	233818.05	0.9291470
Group9-Group8	75272.941	-91250.80	241796.68	0.8712162

Table A13: Tukey data for Stretch

	diff	lwr	upr	p adj
Group1-Group0	2.52377909	-6.591706	11.639264	0.9939302
Group2-Group0	0.22745850	-8.888026	9.342943	1.0000000
Group3-Group0	-3.83381197	-13.502244	5.834620	0.9363865
Group4-Group0	-0.49283923	-11.018494	10.032816	1.0000000
Group5-Group0	0.80427487	-8.311210	9.919760	0.9999995
Group6-Group0	-2.07149832	-11.186983	7.043986	0.9986211
Group7-Group0	-1.84324683	-11.511679	7.825185	0.9996581
Group8-Group0	0.17627477	-9.492157	9.844706	1.0000000
Group9-Group0	0.14497230	-9.523459	9.813404	1.0000000
Group2-Group1	-2.29632059	-11.411805	6.819164	0.9969725
Group3-Group1	-6.35759106	-16.026023	3.310841	0.4613125
Group4-Group1	-3.01661832	-13.542274	7.509037	0.9922254
Group5-Group1	-1.71950422	-10.834989	7.395981	0.9996863
Group6-Group1	-4.59527741	-13.710762	4.520207	0.7853534
Group7-Group1	-4.36702592	-14.035458	5.301406	0.8717107
Group8-Group1	-2.34750432	-12.015936	7.320927	0.9977077
Group9-Group1	-2.37880679	-12.047238	7.289625	0.9974655
Group3-Group2	-4.06127047	-13.729702	5.607161	0.9122207

Group4-Group2	-0.72029773	-11.245953	9.805358	0.9999999
Group5-Group2	0.57681637	-8.538668	9.692301	1.0000000
Group6-Group2	-2.29895682	-11.414442	6.816528	0.9969463
Group7-Group2	-2.07070533	-11.739137	7.597726	0.9991328
Group8-Group2	-0.05118373	-9.719615	9.617248	1.0000000
Group9-Group2	-0.08248620	-9.750918	9.585945	1.0000000
Group4-Group3	3.34097275	-7.667021	14.348966	0.9883793
Group5-Group3	4.63808684	-5.030345	14.306519	0.8283118
Group6-Group3	1.76231365	-7.906118	11.430745	0.9997628
Group7-Group3	1.99056515	-8.200857	12.181987	0.9995842
Group8-Group3	4.01008675	-6.181335	14.201509	0.9391550
Group9-Group3	3.97878428	-6.212638	14.170206	0.9418578
Group5-Group4	1.29711410	-9.228541	11.822769	0.9999912
Group6-Group4	-1.57865910	-12.104314	8.946996	0.9999531
Group7-Group4	-1.35040760	-12.358401	9.657586	0.9999916
Group8-Group4	0.66911400	-10.338880	11.677108	1.0000000
Group9-Group4	0.63781153	-10.370182	11.645805	1.0000000
Group6-Group5	-2.87577319	-11.991258	6.239712	0.9848575
Group7-Group5	-2.64752170	-12.315953	7.020910	0.9943958
Group8-Group5	-0.62800010	-10.296432	9.040432	1.0000000
Group9-Group5	-0.65930257	-10.327734	9.009129	1.0000000
Group7-Group6	0.22825150	-9.440180	9.896683	1.0000000
Group8-Group6	2.24777310	-7.420659	11.916205	0.9983556
Group9-Group6	2.21647063	-7.451961	11.884902	0.9985243
Group8-Group7	2.01952160	-8.171900	12.210943	0.9995330
Group9-Group7	1.98821913	-8.203203	12.179641	0.9995882
Group9-Group8	-0.03130247	-10.222724	10.160119	1.0000000

6.2 Appendix B: Full Procedure for obtaining processed results in R

1. Arrange data as .csv files by Sample, Data, and Group, as shown in Table B1 for both stress and stretch as two different files. Place these files in the R working directory or change the R working directory to location of the files using `setwd()`. Make sure the .csv files are using a comma separator, otherwise read.csv requires an additional parameter to parse the separation character correctly.
2. Load each data set into R using `stress <- read.csv("stress.csv")` and `stretch <- read.csv("stretch.csv")`
3. Conduct ANOVA using `stress.aov <- aov(Data ~ Group, data=stress)` and `stretch.aov <- aov(Data ~ Group, data=stretch)`
4. Because the data is unbalanced, an additional ANOVA functions must be used to get the correct p-values. Load the car library with `library(car)`, installing if needed, then use `stress.aov2 <- Anova(stress.aov, type=3)` and `stretch.aov2 <- Anova(stretch.aov, type=3)`

5. Get ANOVA summary data with `stress.aov2` and `stretch.aov2` and copy to a separate document. The `summary()` function can be used as well, however note that the data is separated into quadrants in that case, adding additional fields that were not used in the analysis.
6. Get Tukey output with `TukeyHSD(stress.aov, which = "Group")` and `TukeyHSD(stretch.aov, which="Group")` and copy to a separate document

Table B1: Sample Rows of Stress (left) and Stretch (right) .csv files

Sample	Data	Group
1	2.50E+05	Group0
2	2.22E+05	Group0
3	1.69E+05	Group0
4	1.80E+05	Group0
5	1.41E+05	Group0
1	1.95E+05	Group1
2	2.03E+05	Group1
3	2.57E+05	Group1
4	2.38E+05	Group1
5	1.95E+05	Group1
1	4.14E+05	Group2
2	2.12E+05	Group2
3	2.33E+05	Group2
4	1.57E+05	Group2
5	1.16E+05	Group2
1	8.76E+04	Group3
2	1.71E+05	Group3
3	1.36E+05	Group3
4	1.91E+05	Group3

Sample	Data	Group
1	2.90E+01	Group0
2	2.07E+01	Group0
3	7.79E+00	Group0
4	1.17E+01	Group0
5	1.44E+01	Group0
1	1.89E+01	Group1
2	1.84E+01	Group1
3	1.86E+01	Group1
4	2.03E+01	Group1
5	2.00E+01	Group1
1	1.95E+01	Group2
2	1.73E+01	Group2
3	1.90E+01	Group2
4	1.55E+01	Group2
5	1.33E+01	Group2
1	1.09E+01	Group3
2	1.22E+01	Group3
3	1.16E+01	Group3
4	1.69E+01	Group3

7.0 Bibliography

1: Centers for Disease Control and Prevention, National Center for Health Statistics, Underlying Cause of Death 1999-2017 on CDC WONDER Online Database, 2018

2: Q. Lu, K. Ganesan, D. Simionescu, N. Vyavahare, Novel Porous Aortic Elastin and Collagen Scaffolds for Tissue Engineering, 2003

3: M. DeBakey, A. Goto, The Living Heart, 1977

4: N. Campbell, J. Reese, Biology, 8th Edition, 2008

5: J. Humphrey, Cardiovascular Solid Mechanics: Cells, Tissues, and Organs, 2002

6: C. Molnar, J. Gair, Concepts of Biology, 1st Canadian Edition, 2013

7: R. Stocker, J.F. Keaney Jr., New Insights in Oxidative Stress in the Artery Wall, 2005

8: M. A. Haralson, J. R. Hassell, Extracellular Matrix: A Practical Approach, 1995

9: M. B. Mathews, Connective Tissue: Macromolecular Structure and Evolution, 1975

10: R. Pankov, K. Yamada, Fibronectin at a Glance, 2002

11: D. Mosher, Fibronectin, 1989

12: R. Timpl, H. Rohde, P. Robey, S. Rennard, J.M. Foidart, G. Martin, Laminin - A Glycoprotein from Basement Membranes, 1979

13: H. Lodish, A. Berk, S.L. Zipursky, Molecular Cell Biology. 4th edition., 2000

14: M. Cescon, F. Gattazzo, P. Chen, P. Bonaldo, Collagen VI at a Glance, 2015

15: C. A. Shuttleworth, Type VIII Collagen, 1997

16: J. Fitzgerald, P. Holden, U. Hansen, The expanded collagen VI family: new chains and new questions, 2013

17: C. Kielty, C. Baldock, D. Lee, M. Rock, J. Ashworth, C. Shuttleworth, Fibrillin: From Microfibril Assembly to Biomechanical Function, 2002

18: M. Carmo, L. Colombo, A. Bruno, F. Corsi, L. Roncoroni, M. Cuttin, F. Radice, E. Mussini, P. Settembrini, Alteration of Elastin, Collagen and their Cross-links in Abdominal Aortic Aneurysms, 2002

19: P. Farand, A. Garon, G. Plante, Structure of large arteries: Orientation of elastin in rabbit aortic internalelastic lamina and in the elastic lamellae of aortic media, 2006

20: N. Gundiah, M. B. Ratcliffe, L. A. Pruitt, The Biomechanics of Arterial Elastin, 2008

21: R. Mecham, Methods in Elastic Tissue Biology: Elastin Isolation and Purification, 2008

22: E. Stephen, A. Venkatasubramaniam, T. Good, L.D.T. Topoleski, The Effect of Oxidation on the Mechanical Response and Microstructure of Porcine Aortas, 2013

23: J. Washington III, A Study of the Effects of Oxidation and Glycation on the Cyclic Loading Response of Isolated Arterial Elastin, 2015

24: M, Lu, E. Hansen, Hydrogen Peroxide Wound Irrigation in Orthopaedic Surgery, 2017

25: M. Sulieman, M. Addy, E. MacDonald, J.S. Rees, The effect of hydrogen peroxide concentration on the outcome of tooth whitening: an in vitro study, 2004

26: M. V. Urban, T. Rath, C. Radtke, Hydrogen peroxide (H2O2): a review of its use in surgery, 2017

27: M. Murphy, How mitochondria produce reactive oxygen species, 2009

28: M. Rojkind, J.-A. Domínguez-Rosales, N. Nieto, P. Greenwel, Role of hydrogen peroxide and oxidative stress in healing responses, 2002

29: C. Winterbourn, Toxicity of iron and hydrogen peroxide: the Fenton reaction, 1995

30: L. Pham-Huy, H. He, C. Pham-Huy, Free Radicals, Antioxidants in Disease and Health, 2008

31: S. Ballinger, C. Patterson, C.N. Yan, R. Doan, D. Burow, C. Young, F. M. Yakes, B. Van Houten, C. Ballinger, B. Freeman, M. Runge, Hydrogen Peroxide– and Peroxynitrite-Induced Mitochondrial DNA Damage and Dysfunction in Vascular Endothelial and Smooth Muscle Cells, 2000

32: L.D.T. Topoleski, N.V. Salunke, J. Humphrey, W. Mergner, Composition- and history-dependent radial compressive behavior of human atherosclerotic plaque, 1997

33: R Development Core Team, R Manuals, 2018, https://cran.r-project.org/manuals.html

34: J. M. Bland, D. Altman, Measuring agreement in method comparison studies, 1999

35: N. Madamanchi, A. Vendrov, M. Runge, Oxidative Stress and Vascular Disease, 2005

36: Honeywell International Inc., Model 31 Mid Datasheet, 2012